IEEE Access
Multidisciplinary | Rapid Review | Open Access Journal

Received August 10, 2020, accepted August 14, 2020, date of current version August 17, 2020.

Digital Object Identifier (TBD)

Simultaneous Provision of Voltage and Frequency Control by PV-Battery Systems

HAMADA ALMASALMA, (Member, IEEE) and GEERT DECONINCK, (Senior Member, IEEE)
Departement Elektrotechniek, KU Leuven, Kasteelpark Arenberg 10, 3001 Leuven, Belgium.
EnergyVille Research Center, Thor Park 8310, 3600 Genk, Belgium.

Corresponding author: Hamada Almasalma (e-mail: hamada.almasalma@kuleuven.be).

This research is supported by an SB PhD fellowship from FWO Vlaanderen.

ABSTRACT

With the rise of distributed energy resources, photovoltaic-battery systems are needed to maintain voltages within limits, and balance between demand and supply. These systems can be exploited more by controlling them to provide multiple, stacked services. In this paper, we propose a novel control methodology for photovoltaic-battery systems to provide simultaneously distributed voltage control and frequency containment reserve. The control methodology is structured in two phases. In the day-ahead phase, the control problem is formulated as a robust optimization problem. The aims of this optimization problem are to allocate fractions of the energy and power capacity of each battery energy storage system to the two services, minimize the expected cost of reactive power compensation and batteries degradation, maximize profits from frequency control, and compute a set of linear control policies. The optimization problem also aims to immunize against service unavailability, and violating operational limits. This immunity is accomplished by considering the uncertainty in the households' active power consumption, photovoltaic power generation, and grid frequency. In the real time phase, the linear policies are applied to regulate voltage profiles, and keep energy contents of batteries within limits while providing frequency control. A 120-node low voltage network is used as a case study. Simulations over 10^4 scenarios are used to demonstrate the robustness of the proposed control methodology.

INDEX TERMS Battery energy storage system, smart inverter, distributed voltage control, frequency containment reserve, value stacking, linear policies, robust optimization.

I. INTRODUCTION

Solar photovoltaic (PV) has experienced exponential growth in recent years, with global installed capacity increasing tenfold from 2010 to 2019 [1]. It is also predicted that the global PV capacity will continue to grow by 9% every year in the next 50 years [2]. The market for battery energy storage systems is expected to grow at a compound annual growth rate of approximately 50% during the period 2020-2025 [3]. This transition towards distributed energy resources (DERs) is impacting the operation of distribution networks [4]. Distribution networks were originally designed as passive networks, containing mainly loads. Therefore, a high penetration of DERs leads to several technical challenges in controlling distribution networks. One of the main problems is voltage rise issue due to the feed-in power from DERs [5]. Furthermore, intermittent and unpredictable nature of PV systems increases the complexity of balancing the grid.

Smart PV-battery systems with advanced grid support mechanisms and data communication capabilities are being deployed to tackle the negative impact of increased DERs penetration on grid voltage and frequency [6]. These systems have the ability to absorb (or inject) reactive power, curtail PV power, charge battery energy storage systems (BESSs) during PV peak period and discharge BESSs during demand peak period. Additionally, their energy output can be controlled in response to frequency deviations.

Since frequency control has been identified as one of the highest value services for PV-battery systems [7], many researchers are interested in using these systems to provide frequency control service to the grid. These systems can

This article has been accepted for publication in a future issue of this journal, but has not been fully edited. Content may change prior to final publication. Citation information: DOI 10.1109/ACCESS.2020.3018086, IEEE Access

be exploited more by controlling them to provide multiple, stacked services along with the frequency control service. Optimizing the deployment of PV-battery systems to get the most possible value out of them has attracted increasing attention recently [8]. Different control methodologies have been proposed in literature that allow PV-battery systems to combine frequency control with different services, such as increasing self-consumption and peak shaving.

Providing frequency control (along with other services) with PV-battery systems connected to the low voltage distribution grid can lead to voltage issues [9]. In order to mitigate these issues, part of the reserve capacity of the PV-battery systems should be dedicated to solve voltage problems caused by their services. In the opinion of the authors, grid operators should require frequency control providers (with PV-battery systems located in distribution networks) to provide frequency control simultaneously with voltage control.

There is no study that has actually been carried out to design and optimize controllers that allow PV-battery systems to combine frequency control with voltage control; this is the literature gap that our study seeks to fill and the motivation of this paper.

To enable PV-battery systems to actively participate in voltage regulation, various voltage control strategies of different complexity and data transfer needs have been proposed in literature. One of the effective control strategies that enables smart inverters of the PV-battery systems to regulate grid voltage is distributed coordinated voltage control (DisCVC) [10]. In DisCVC, smart inverters communicate with each other in a peer-to-peer (P2P) fashion to solve a voltage control problem in a distributed way without relying on a central decision-making controller.

The main contributions of this paper are:

- We propose an optimized controller that allows PV-battery systems to provide simultaneously DisCVC and frequency containment reserve (FCR).
- We propose upward and downward energy management policies that regulate energy content of BESSs within limits while providing FCR.
- We propose a novel DisCVC system enabled by reactive and active power policies.
- We propose a new design for the upward and downward reserve capacity profiles.

The remainder of the paper is organised as follows: section II presents a background on provision of FCR with BESSs. Related literature is reviewed in section III. Section IV presents a general overview of the proposed control system. The optimization problem treated in this paper is formulated in section V. Results that validate the proposed mathematical optimization problem are presented in section VI. Finally, the paper is concluded in section VII and some suggestions for future work are given.

II. PROVISION OF FREQUENCY CONTAINMENT RESERVE WITH A BESS

The objective of the FCR is to maintain active power balance between consumption and generation, within a synchronous area, at a frequency close to the nominal frequency f_{nom}. FCR reserve capacity is activated automatically in response to the grid frequency deviations from the nominal frequency. FCR is the fastest reserve procured by transmission system operators (TSOs); providers are required to reach their full committed reserve capacity within 30 seconds. In many countries, TSOs procure their FCR capacity via a periodic auctions in which third parties, such as aggregators, can bid a certain amount of reserve capacity at a certain price. When accepted, the committed FCR capacity should be provided continuously with 100% availability during the contracted period [11]. Until the middle of 2019, FCR auctions in Europe were put out on a weekly basis. From July of 2019, the contracted period was reduced from one week to one day. This shortened period will help FCR providers to design their control systems in a more robust way, as uncertainty is considered for only one day [12].

The FCR power $p_{\text{FCR}}^{(k)}$ of a certain asset, participating in frequency control, should be adjusted proportional to the relative grid frequency deviations, as shown in (1a) [1].

$$p_{\text{FCR}}^{(k)} = r\Delta f^{(k)}, \tag{1a}$$

$$\Delta f^{(k)} = \begin{cases} \frac{f^{(k)} - f_{\text{nom}}}{\overline{\Delta f}} & \text{if } \Delta f_{\text{db}} < \mid f^{(k)} - f_{\text{nom}} \mid < \overline{\Delta f}, \\ 1 & \text{if } f^{(k)} - f_{\text{nom}} \geq \overline{\Delta f}, \\ -1 & \text{if } f^{(k)} - f_{\text{nom}} \leq -\overline{\Delta f}, \\ 0 & \text{otherwise.} \end{cases} \tag{1b}$$

Here, k is the time step of the frequency control, $\overline{\Delta f}$ is the frequency deviation at which maximum FCR capacity r needs to be activated, and Δf_{db} is the frequency deadband in which no FCR reaction is required. In the Continental Europe (CE) synchronous area, $\overline{\Delta f} = 200$ mHz and $\Delta f_{\text{db}} = 10$ mHz.

Non-delivery or non-availability of a committed FCR reserve capacity will result in penalties charged by the TSO. Providers can lose all revenues made from FCR in case of not meeting the FCR requirements, or can be excluded from further participation in the market in case delivery is consistently not available or insufficient.

As BESSs have proven great potential in providing FCR [9], many TSOs opened their networks for BESSs and released new FCR regulations for assets with limited energy reservoirs [13]. BESSs are expected to entirely take over the role of FCR providers from thermal power plants. Nevertheless, designing a control system that enables BESSs to provide FCR is not straightforward. Due to the limited capacity of batteries, ensuring the FCR reserve capacity r is

[1]The convention in this paper is that the power is positive when it is consumed (e.g., charging power of the BESS) and negative when it is injected (e.g., discharging power of the BESS).

This article has been accepted for publication in a future issue of this journal, but has not been fully edited. Content may change prior to final publication. Citation information: DOI 10.1109/ACCESS.2020.3018086, IEEE Access

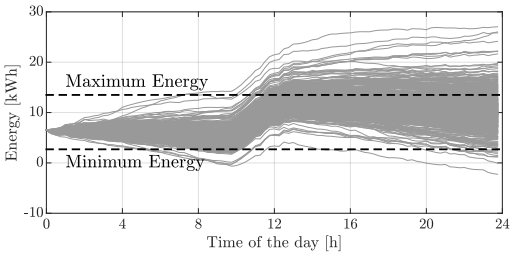

Fig. 1: Energy content of the 13.5 kWh battery over 730 frequency scenarios. Battery parameters: maximum power= 7 kW, initial charge= 6.5 kWh, charge/discharge efficiency= $\sqrt{0.9}$. The energy content E is calculated based on: $E^{(k+1)} = E^{(k)} + \Delta t \left(\eta_i^{\text{ch}} \left[p_{\text{FCR}}^{(k)} \right]^+ - \frac{1}{\eta_i^{\text{dis}}} \left[-p_{\text{FCR}}^{(k)} \right]^+ \right)$, where η_i^{ch} and η_i^{dis} are, respectively, the charge and discharge efficiencies , Δt is the time step duration (1 minute) and $[\cdot]^+ \equiv \max(\cdot, 0)$.

available during the contracted period is not possible without a management strategy that keeps energy content of BESSs within limits. This is because the frequency signal has a non-zero energy content over short time periods, and efficiency losses of batteries decrease their energy content when being charged or discharged. Fig. 1 demonstrates the fact that a BESS cannot be used to provide FCR without an energy management strategy. In Fig. 1, a 13.5 kWh residential battery is used to provide FCR based on (1a). Two years of frequency data (2017-2018) with 1 minute resolution, from the CE synchronous region [14], are used to study the energy content of the 13.5 kWh battery while providing FCR. One can clearly notice the violation of the maximum and minimum energy content limits. Hence, an energy management strategy is a must.

The German TSOs have defined control strategies [15], also referred to as degrees of freedom (Dof), which can be utilized to keep energy content of batteries within operational range during FCR provision. These strategies presume that BESSs can deviate slightly from the required FCR Power. These strategies are: 1) overdelivery: providers are allowed to provide FCR power that is anywhere between 100% and 120% of the instantaneous FCR requirement, 2) deadband utilization: usually FCR assets are not obliged to activate their reserve capacity within the range ± 10 mHz around the nominal frequency, a battery can use this deadband for charging and discharging by using a power within the range $\left[0, p_{\text{FCR}}^{(k)}\right]$ in case of charging, or within the range $\left[-p_{\text{FCR}}^{(k)}, 0\right]$ in case of discharging. A comparison of these control strategies is made in [15], in which authors conclude that overdelivery and deadband utilization are not sufficient to regulate the energy contents of BESSs within limits while providing FCR. Providers, who wish to use these strategies, should combine them with an additional management strategy, or use a single battery management strategy that can regulate energy content of batteries within limits while providing FCR.

III. RELATED WORK

A. BATTERIES PROVIDING MULTIPLE SERVICES

BESSs create value for prosumers and grid operators, but leave significant untapped value on the table. Currently, most BESSs are deployed for one of three single applications: maximization of PV self-consumption, demand charge reduction, or backup power. This results in batteries sitting unused for over half of their lifetime [16]. Hence, there is a need for designing innovative control systems that enable batteries to provide simultaneously multiple services (so-called value stacking). The challenges of designing such a control system are to decide how much of batteries' energy and power capacities to allocate to each service, minimize the risk of service unavailability, and minimize the risk of violating battery constraints.

A control framework is designed in [17] for a BESS to provide simultaneously FCR and dispatch of the operation of an active distribution feeder. The work of [18] presents a methodology for evaluating benefits of batteries for multiple services, including balancing service, energy arbitrage, distribution system equipment deferral, and power outage mitigation. Model predictive control is used in [19] to dynamically co-optimize the allocation of batteries energy and power capacities over three services: FCR, minimization of PV curtailment, and demand smoothing. A dynamic programming approach is applied in [20] to co-optimize a storage device for energy arbitrage and frequency regulation. A joint optimization framework is proposed in [21] for batteries to perform peak shaving and provide frequency regulation service. Stochastic dual dynamic programming is applied in [22] to implement a control system that enables PV-battery systems to provide FCR, automatic frequency restoration reserve (aFRR), and maximization of PV self-consumption. A controller that allows batteries to be used simultaneously for self-consumption and FCR is presented in [23], stochastic and robust optimization techniques are used to maximize the expected profit from combining these two services, the controller also computes a linear management policy that regulates battery energy content within limits while providing FCR.

To the best of our knowledge, simultaneous provision of voltage control and FCR by BESSs has not been discussed in literature yet. The novel control system proposed in this paper combines FCR with a policy-based distributed voltage control system, to enable PV-battery systems to provide simultaneously voltage and frequency control. Below, we present a brief literature review on policy-based voltage control techniques, that we extend to build a policy-based distributed voltage control system.

B. POLICY-BASED DISTRIBUTED VOLTAGE CONTROL

Various approaches that combine local, centralized and distributed voltage control techniques have been proposed in literature [24]. These techniques suffer from different problems; centralized voltage control incurs high computational complexity; most of distributed voltage control techniques require large number of iterations to converge; and local voltage control has no performance guarantees. As a middle-ground solution, a centralized coordinator can be run on an offline basis (i.e. day-ahead) to compute voltage control

This article has been accepted for publication in a future issue of this journal, but has not been fully edited. Content may change prior to final publication. Citation information: DOI 10.1109/ACCESS.2020.3018086, IEEE Access

policies. A distributed voltage control can then be applied in real time enabled by the computed control policies. The idea is to let PV-battery systems solve, each time step in real time, a set of linear equations rather than solving a complex optimization problem. In [25]–[28], different techniques are used for computing linear voltage control policies: chance constrained programming in [25]; distributionally robust chance constraints in [26]; affinely adjustable robust optimization in [27]; and conic robust optimization in [28]. The aforementioned control policies are designed for local voltage control, they are not meant for coordinated voltage control. The voltage control methodology developed in [29] builds on the techniques presented in [25]–[28], but extends the voltage control policies to be used for enabling real time distributed voltage control. This paper extends the robust optimization problem of [29] to combine policy-based distributed voltage control with frequency control.

IV. GENERAL OVERVIEW OF THE PROPOSED CONTROL FRAMEWORK

We propose a robust optimization-based control framework for PV-battery systems to simultaneously provide policy-based DisCVC and FCR. General overview of the proposed control framework is shown in Fig. 2. The control framework consists of two phases. In the day-ahead phase, the combined voltage and frequency control problem is formulated as a robust optimization problem. The aims of this optimization problem are to allocate fractions of the energy and power capacity of each BESS to the two services, compute a set of linear control policies (voltage control policies and battery management policies), minimize the expected cost of reactive power compensation and batteries degradation cost, and maximize profits from FCR. The robust optimization problem also aims to immunize against service unavailability, and violating batteries, inverters and voltage constraints. This immunity is accomplished by considering the uncertainty in the households' active power consumption, PV power generation, and grid frequency.

In the real time phase, the grid support functions of smart PV-battery inverters apply the linear control policies to regulate voltage profiles, and keep energy content of BESSs within limits while providing FCR service. Each battery is divided into 3 virtual batteries: voltage control battery (VC battery) that regulates grid voltage together with the inverter reactive power; upward-FCR battery (R-UP battery) that provides upward frequency regulation; and downward-FCR battery (R-DN battery) that provides downward frequency regulation. Each inverter contains two grid support functions, grid voltage support function (GVSF) and frequency support function (FSF). The GVSF hosts two voltage control policies: reactive power policy that gives reactive power setpoints of the inverter, and active power policy that gives setpoints of the VC battery power. As designing a voltage control policy based only on local information yields to a poor performance [30], each voltage control policy is designed as a linear function of the local active powers of the household's load and PV installation, and active powers of the households' loads and PV installations connected to the nodes participating in voltage control (control nodes). Each GVSF needs to know the sum of the households' active power consumption and PV power generation of the nodes participating in voltage control, to be able to compute its own control actions. To compute the sum of the households' active power consumption and PV power generation in a fast and efficient way, a P2P-based push-sum gossip protocol is applied in this paper [31]. The push-sum gossip protocol enables the PV-battery inverters to perform a distributed summation with a moderate communication overhead.

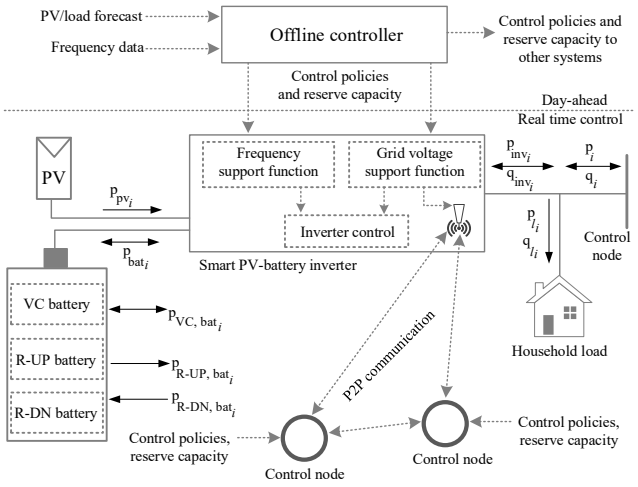

Fig. 2: General overview of the proposed control framework.

The FSF computes the upward-FCR power of the R-UP battery, and the downward-FCR power of the R-DN battery. The FSF hosts two linear management policies: an R-UP battery management policy that maintains energy content of the R-UP battery within limits while providing upward frequency regulation; and an R-DN battery management policy that maintains energy content of the R-DN battery within limits while providing downward frequency regulation.

A. FCR RESERVE CAPACITY

In this work, we consider the case of end-prosumers, with PV-battery systems, providing FCR service to the TSO, possibly through an intermediary, for example an aggregator. In distribution networks with high PV penetration, the FCR capacity is affected by the magnitude of voltages, the capability of the voltage control system, and inverters capacity. Batteries located in a distribution network with a voltage problem cannot commit to provide a fixed reserve capacity over the entire contracted period; they can commit to provide a variable reserve capacity. Moreover, they cannot commit to provide the same reserve capacity for the upward-

This article has been accepted for publication in a future issue of this journal, but has not been fully edited. Content may change prior to final publication. Citation information: DOI 10.1109/ACCESS.2020.3018086, IEEE Access

FCR and downward-FCR[2]. Hence, we propose a variable FCR capacity profile. The FCR is proposed to be auctioned daily in the form of 15 minutes products. The upward and downward reserves are proposed to be procured independently. Prosumers (or their aggregator) shall send day-ahead two FCR profiles to the TSO: upward-FCR capacity profile; and downward-FCR capacity profile. The example of Fig. 3 shows the reason why we propose a variable FCR capacity for batteries located in distribution networks with voltage problems.

Fig. 3a shows a voltage profile of a prosumer, with a PV-battery system, located in a distribution network with high feed-in power from PV installations; Fig 3b shows the expected upward and downward reserve capacity profiles of the prosumer's battery that provide simultaneously voltage and frequency control. If the amount of available reactive power capacity is sufficient to solve the voltage rise problem (of Area 2 in Fig. 3a) without the need to charge the VC battery, the R-UP battery can be discharged to provide upward-FCR. In this case, the upward-FCR capacity depends on the amount of remaining reactive power capacity that can support the R-UP battery to inject more FCR power without causing the network violating voltage operation limits. On the other hand, if the amount of available reactive power capacity is not sufficient to solve the voltage rise problem, the controller will charge the VC battery. In this case, the R-UP battery cannot be discharged to provide upward-FCR[3], as the battery[4] cannot be charged and discharged at the same time. Since there is no voltage rise problem in Area 1 and Area 3, the R-UP battery can be discharged in these areas to provide upward-FCR. The voltage in Area 1 is closer to the maximum limit than the voltage in Area 3, therefore, the upward-FCR capacity in Area 1 is expected to be less than the upward-FCR capacity in Area 3.

As there is no voltage drop problem in the example of Fig. 3, the R-DN battery can be charged in the three areas to provide downward-FCR. The downward-FCR capacity depends on the amount of reactive power capacity that can support the R-DN battery to absorb more FCR power without causing the network violating voltage operation limits. In Area 2 of Fig. 3a, the downward-FCR capacity is expected to be at minimum, since most of the inverter capacity is expected to be occupied by the PV power and the reactive power of the voltage control system. The downward-FCR capacity in Area 3 is expected to be less than the downward-FCR capacity in Area 1. This is because the voltage in Area 3 is closer to the minimum voltage limit than the voltage in Area 1.

[2]In the upward-FCR, batteries are discharged in response to the negative frequency deviation, whereas in the downward-FCR, batteries are charged in response to the positive frequency deviation.

[3]It is worth to point out that the priority of the control system is to solve voltage rise problems. This is to avoid inverters disconnection due to overvoltage.

[4]In this paper, if the word "battery" is not preceded by the three abbreviations: VC; R-UP; and R-DN, then this word means the real battery and not one of the three virtual batteries.

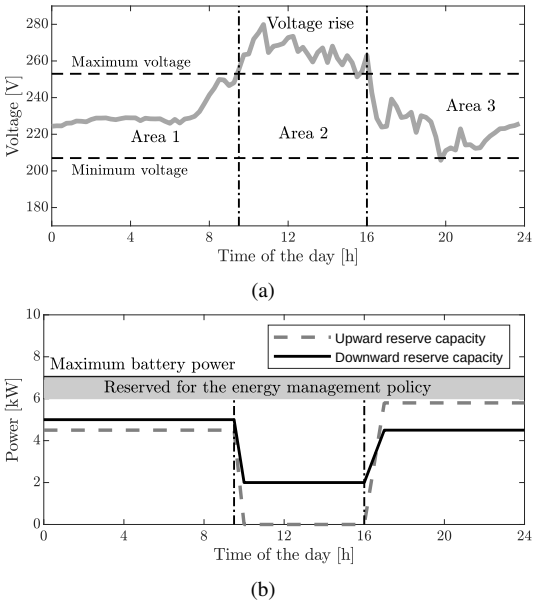

FIGURE 3: (a) Unregulated voltage profile of a prosumer in a network with high PV penetration, (b) Expected upward and downward reserve capacity profile. In this example, the inverter reactive power and the VC battery charging power are used to solve the voltage rise problem, therefore, the upward reserve capacity is zero in Area 2.

For sake of simplicity, the power capacity reserved for the energy management policy of the example of Fig. 3b is set to a constant value of 1 kW. In the proposed optimization problem, the power capacity of the energy management policy is considered as a variable capacity to compute the minimum sufficient power capacity. It is clear from Fig. 3b that the energy management policy will have to be designed carefully, as more power capacity for the management policy will mean that less FCR capacity can be sold to the TSO, while on the other hand the power capacity for the management policy should be sufficient to ensure the energy content of the battery remains within limits.

V. PROBLEM FORMULATION

In this section, we design the models needed to build the problem the offline controller solves on a day-ahead basis. The uncertainty model (that will be discussed in subsection V-A) is used to handle uncertainties in demand, PV generation and grid frequency. The models of batteries, inverters and branch flow (that will be discussed in subsections V-D, V-E and V-F) are used to define the operational limits of the PV-battery systems and grid voltage. The power and energy allocation models (that will be designed in subsection V-C) are used to allocate fractions of the energy and power capacity of each BESS to the voltage and frequency control services. The logic constraints (that will be formulated in subsection V-G) are used to avoid conflict between voltage and frequency control (i.e., charging and discharging a battery at the same time). The objective function (that will be formulated in subsection V-H) is used to minimize the expected cost of operating the voltage control system and maximize profits from FCR. The robust optimization problem

This article has been accepted for publication in a future issue of this journal, but has not been fully edited. Content may change prior to final publication. Citation information: DOI 10.1109/ACCESS.2020.3018086, IEEE Access

(that will be formulated in subsection V-I) is designed based on the aforementioned models; it computes the coefficients of the linear control policies (that will be designed in subsection V-B) and the upward/downward reserve capacity profiles.

The time horizon of the optimization problem is one day, discretized into n_t time steps of duration Δt. The time steps belong to the set $\mathcal{K} = \{1, \cdots, n_t\}$.

We consider two types of network's nodes: control nodes where the PV-battery inverters and households' loads are connected; and passive nodes with only households' loads. Control nodes belong to the set $\mathcal{I} = \{1, \cdots, n_c\}$, passive nodes belong to the set $\mathcal{J}$, and network's nodes belong to the set $\mathcal{N} = \{1, \cdots, n_{\text{nodes}}\}$. n_c is the number of control nodes, and n_{nodes} is the number of network's nodes. A tilde sign ($\sim$) is used in this paper to indicate a variable subject to uncertainty.

A. UNCERTAINTY MODEL

The sources of uncertainty in the control problem of the offline controller include households' active and reactive power consumption, PV power generation, and the grid frequency. The uncertain household's active power consumption $\tilde{p}_{l_x}^{(k)}$, and the uncertain PV power generation $\tilde{p}_{\text{pv}_i}^{(k)}$ can be bounded as:

$$\left.\begin{aligned} &0 \le \tilde{p}_{l_x}^{(k)} \le \overline{p}_{l_x}^{(k)} \\ &\overline{p}_{l_x}^{(k)} = p_{l_x}^{(k)} + \Delta p_{l_x}^{(k)} \end{aligned}\right\} \forall x \in \mathcal{N}, \forall k \in \mathcal{K} \tag{2}$$

$$\left.\begin{aligned} &0 \le \tilde{p}_{\text{pv}_i}^{(k)} \le \overline{p}_{\text{pv}_i}^{(k)} \\ &\overline{p}_{\text{pv}_i}^{(k)} = p_{\text{pv}_i}^{(k)} + \Delta p_{\text{pv}_i}^{(k)} \end{aligned}\right\} \forall i \in \mathcal{I}, \forall k \in \mathcal{K} \tag{3}$$

Where $\overline{p}_{l_x}^{(k)}$ and $\overline{p}_{\text{pv}_i}^{(k)}$ are, respectively, the maximum uncertain household's active power consumption, and the maximum uncertain PV power generation. $\overline{p}_{l_x}^{(k)}$ is defined in (2) as the sum of the forecasted household's active power consumption $p_{l_x}^{(k)} \in \mathbb{R}_{\ge 0}$ and the maximum deviation $\Delta p_{l_x}^{(k)}$ from the forecast of the household's active power consumption. In (3), $\overline{p}_{\text{pv}_i}^{(k)}$ is defined as the sum of the forecasted PV power generation $p_{\text{pv}_i}^{(k)} \in \mathbb{R}_{\ge 0}$ and the maximum deviation $\Delta p_{\text{pv}_i}^{(k)}$ from the PV forecast. $\Delta p_{l_x}^{(k)}$ and $\Delta p_{\text{pv}_i}^{(k)}$ can be approximated based on historical data of forecast error.

The uncertain household's reactive power consumption $\tilde{q}_{l_x}^{(k)}$ can be defined as function of $\tilde{p}_{l_x}^{(k)}$ and a power factor (PF):

$$\tilde{q}_{l_x}^{(k)} = \tan\left(\text{acos}\left(\text{PF}\right)\right) \tilde{p}_{l_x}^{(k)}, \forall x \in \mathcal{N}, \ \forall k \in \mathcal{K} \tag{4}$$

A normalized positive frequency deviation $\widetilde{\Delta f}_{\text{R-DN}}^{(k)}$ (related to the downward-FCR), and normalized negative frequency deviation $\widetilde{\Delta f}_{\text{R-UP}}^{(k)}$ (related to the upward-FCR) can be bounded as:

$$0 \le \widetilde{\Delta f}_{\text{R-DN}}^{(k)} \le \overline{\Delta f}_{\text{R-DN}}^{(k)}, \forall k \in \mathcal{K} \tag{5a}$$

$$\underline{\Delta f}_{\text{R-UP}}^{(k)} \le \widetilde{\Delta f}_{\text{R-UP}}^{(k)} \le 0, \forall k \in \mathcal{K} \tag{5b}$$

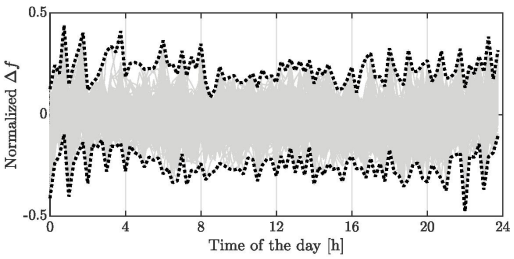

Fig. 4: Normalized positive and negative frequency deviation Δf of 730 days of historical frequency data (2017-2018). The dotted lines show the maximum and minimum normalized frequency deviation. Δf is calculated based on (1b). The frequency data are from the CE synchronous region [14].

Here, $\overline{\Delta f}_{\text{R-DN}}^{(k)}$ and $\underline{\Delta f}_{\text{R-UP}}^{(k)}$ are the maximum normalized frequency deviation and minimum normalized frequency deviation at time step k, respectively. In this paper, $\overline{\Delta f}_{\text{R-DN}}^{(k)}$ and $\underline{\Delta f}_{\text{R-UP}}^{(k)}$ are set based on historical frequency data. One can set $\overline{\Delta f}_{\text{R-DN}}^{(k)}$ to 1, and $\underline{\Delta f}_{\text{R-UP}}^{(k)}$ to $-1 \ \forall k \in \mathcal{K}$, which is correct. However, from our experience, this will lead to conservative solutions, e.g., low contracted reserve capacity. As shown in Fig. 4, the historical maximum normalized frequency deviation can be much less than 1, and the historical minimum normalized frequency deviation can be much higher than -1.

For given historical frequency measurements with n_f measurements per time step k, $\overline{\Delta f}_{\text{R-DN}}^{(k)}$ and $\underline{\Delta f}_{\text{R-UP}}^{(k)}$ can be calculated as:

$$\left(\Delta f^{(k)}\right)^{(\varkappa)} = \tag{6}$$

$$\begin{cases} \frac{(f^{(k)})^{(\varkappa)} - f_{\text{nom}}}{\overline{\Delta f}} & \text{if } \Delta f_{\text{db}} < \mid (f^{(k)})^{(\varkappa)} - f_{\text{nom}} \mid < \overline{\Delta f}, \\ 1 & \text{if } (f^{(k)})^{(\varkappa)} - f_{\text{nom}} \ge \overline{\Delta f}, \\ -1 & \text{if } (f^{(k)})^{(\varkappa)} - f_{\text{nom}} \le -\overline{\Delta f}, \\ 0 & \text{otherwise.} \end{cases}$$

$$\varkappa = 1, \cdots, n_f,$$

$$\overline{\Delta f}_{\text{R-DN}}^{(k)} = \max\left(\left[\left(\Delta f^{(k)}\right)^{(1)}\right]^{+}, \cdots, \left[\left(\Delta f^{(k)}\right)^{(n_f)}\right]^{+}\right),$$

$$\underline{\Delta f}_{\text{R-UP}}^{(k)} = \min\left(\left[\left(\Delta f^{(k)}\right)^{(1)}\right]^{-}, \cdots, \left[\left(\Delta f^{(k)}\right)^{(n_f)}\right]^{-}\right)$$

Here, $\left(\Delta f^{(k)}\right)^{(\varkappa)}$ is the normalized frequency deviation number $\varkappa$ related to the frequency measurement number $\varkappa$ $(f^{(k)})^{(\varkappa)}$ at time step k. The operator $[\cdot]^{+} \equiv \max(\cdot, 0)$, and $[\cdot]^{-} \equiv \min(\cdot, 0)$.

To get immunity against service unavailability, and violating operational constraints, we look for solutions which are feasible for any realization of the uncertain data in a predefined uncertainty set $\mathcal{U}$. In this paper, we consider a polyhedral model of the uncertainty set of the form:

$$\mathcal{U} = \{\boldsymbol{\zeta} \ge 0 : \boldsymbol{H}\boldsymbol{\zeta} \le \boldsymbol{h}\}, \tag{7}$$

$\boldsymbol{H} \in \mathbb{R}^{2n_\zeta \times n_\zeta}$ and $\boldsymbol{h} \in \mathbb{R}^{2n_\zeta}$ can be defined to represent the constraints (2)-(5b), where $n_\zeta = n_t(2 + n_c + n_{\text{nodes}})$ is the number of uncertain variables for n_t times steps. The

This article has been accepted for publication in a future issue of this journal, but has not been fully edited. Content may change prior to final publication. Citation information: DOI 10.1109/ACCESS.2020.3018086, IEEE Access

vector $\boldsymbol{\zeta} \in \mathbb{R}^{n_\zeta}$ includes the uncertain households' active power consumption, PV power generation, normalized positive frequency deviations, and normalized negative frequency deviations for n_t time steps:

$$\boldsymbol{\zeta} = \Big[\tilde{\boldsymbol{P}}_l^{(1)}, \cdots, \tilde{\boldsymbol{P}}_l^{(n_t)}, \tilde{\boldsymbol{P}}_{\text{pv}}^{(1)}, \cdots, \tilde{\boldsymbol{P}}_{\text{pv}}^{(n_t)}, \widetilde{\Delta f}_{\text{R-DN}}^{(1)}, \cdots, \widetilde{\Delta f}_{\text{R-DN}}^{(n_t)}, \widetilde{\Delta f}_{\text{R-UP}}^{(1)}, \cdots, \widetilde{\Delta f}_{\text{R-UP}}^{(n_t)}\Big]^T \tag{8a}$$

$$\tilde{\boldsymbol{P}}_l^{(k)} = \Big[\tilde{p}_{l_1}^{(k)}, \cdots, \tilde{p}_{l_{n_{\text{nodes}}}}^{(k)}\Big], \forall k \in \mathcal{K} \tag{8b}$$

$$\tilde{\boldsymbol{P}}_{\text{pv}}^{(k)} = \Big[\tilde{p}_{\text{pv}_1}^{(k)}, \cdots, \tilde{p}_{\text{pv}_{n_c}}^{(k)}\Big], \forall k \in \mathcal{K} \tag{8c}$$

In subsection V-I, we present the robust counterpart formulation of uncertain linear constraints. The robust counterpart formulation is derived based on the uncertainty set $\mathcal{U}$ defined in (7).

The convention in this paper is that the power is positive when it is consumed and negative when it is injected. In (3), $\tilde{p}_{\text{pv}_i}^{(k)}$ and $p_{\text{pv}_i}^{(k)}$ are defined as positive values. Hence, a minus sign will be introduced in front of $\tilde{p}_{\text{pv}_i}^{(k)}$ and $p_{\text{pv}_i}^{(k)}$.

B. LINEAR CONTROL POLICIES

Robust optimization is a technique to solve mathematical optimization problems in which the data are uncertain and are only known to belong to some uncertainty set. The goal of robust optimization is to find solutions that are immune to uncertainty. In static robust optimization, decisions must be made before the realization of the uncertain data. Ben-Tal et al. extended the robust optimization framework to dynamic settings by proposing the adjustable robust optimization (ARO) technique [32], in which some decision variables are allowed to be computed after the realization of the uncertain data, thus leading to better objective value and less conservative solutions. This performance is achieved at higher computational burden, as ARO is usually NP-hard to solve. Ben-Tal et al. proposed the method of affinely adjustable robust optimization (AARO) to construct a tractable optimization problem. In AARO, decision variables are restricted to be affine functions of the uncertain data [33]. Accordingly, control policies proposed in this paper are designed as linear functions of the uncertain data.

As has been discussed in section IV, we consider four linear control policies for each PV-battery system: reactive power policy that gives reactive power setpoints; active power policy that gives charge/discharge power setpoints of the VC battery; R-UP battery management policy that gives charge power setpoints needed to maintain the energy content of the R-UP battery within limits while providing upward-FCR; and R-DN battery management policy that gives discharge power setpoints needed to maintain the energy content of the R-DN battery within limits while providing downward-FCR.

Active and Reactive Power Policies

To regulate voltage profiles, each PV-battery system adjusts its reactive power and VC battery power linearly as function of control nodes' active power consumption and PV power generation, and normalized frequency deviations. Given the possibility that the frequency deviation can be either positive or negative for each time step, we propose two types of reactive power policy: reactive power policy that takes into account the effect of responding to positive frequency deviations; and reactive power policy that takes into account the effect of responding to negative frequency deviations:

$$\forall i \in \mathcal{I}, \forall k \in \mathcal{K}:$$

$$\tilde{q}_{\text{R-DN, inv}_i}^{(k)} = \beta_{\text{p}_i}^{(k)} \sum_{i \in \mathcal{I}} \Big(\tilde{p}_{l_i}^{(k)} - \tilde{p}_{\text{pv}_i}^{(k)}\Big) + \beta_{\text{R-DN}_i}^{(k)} \widetilde{\Delta f}_{\text{R-DN}}^{(k)} \tag{9a}$$

$$\tilde{q}_{\text{R-UP, inv}_i}^{(k)} = \beta_{\text{p}_i}^{(k)} \sum_{i \in \mathcal{I}} \Big(\tilde{p}_{l_i}^{(k)} - \tilde{p}_{\text{pv}_i}^{(k)}\Big) + \beta_{\text{R-UP}_i}^{(k)} \widetilde{\Delta f}_{\text{R-UP}}^{(k)} \tag{9b}$$

where $\tilde{q}_{\text{R-DN, inv}_i}^{(k)}$ and $\tilde{q}_{\text{R-UP, inv}_i}^{(k)}$ are the uncertain reactive powers of inverter i (at time step k) that take into account the effect of downward-FCR and upward-FCR, respectively, on mitigating voltage problem. $\beta_{\text{p}_i}^{(k)}$ is the coefficient of the reactive power policy (of inverter i at time step k) related to the active powers of households' loads and PV installations connected to the control nodes. $\beta_{\text{R-DN}_i}^{(k)}$ and $\beta_{\text{R-UP}_i}^{(k)}$ are, respectively, the coefficients of the reactive power policy related to the positive and negative normalized frequency deviations at time step k. The two types of the reactive power policy can be defined in a vectorized form as:

$$\forall i \in \mathcal{I}:$$

$$\tilde{\boldsymbol{Q}}_{\text{R-DN, inv}_i} = \Big[\tilde{q}_{\text{R-DN, inv}_i}^{(1)}, \cdots, \tilde{q}_{\text{R-DN, inv}_i}^{(n_t)}\Big]^T = \boldsymbol{\beta}_{\text{p}_i} \boldsymbol{\xi}_{\Delta p} + \boldsymbol{\beta}_{\text{R-DN}_i} \boldsymbol{\xi}_{\text{R-DN}} \tag{10a}$$

$$\tilde{\boldsymbol{Q}}_{\text{R-UP, inv}_i} = \Big[\tilde{q}_{\text{R-UP, inv}_i}^{(1)}, \cdots, \tilde{q}_{\text{R-UP, inv}_i}^{(n_t)}\Big]^T = \boldsymbol{\beta}_{\text{p}_i} \boldsymbol{\xi}_{\Delta p} + \boldsymbol{\beta}_{\text{R-UP}_i} \boldsymbol{\xi}_{\text{R-UP}} \tag{10b}$$

$$\boldsymbol{\xi}_{\Delta p} = \left[\sum_{i \in \mathcal{I}} \Big(\tilde{p}_{l_i}^{(1)} - \tilde{p}_{\text{pv}_i}^{(1)}\Big), \cdots, \sum_{i \in \mathcal{I}} \Big(\tilde{p}_{l_i}^{(n_t)} - \tilde{p}_{\text{pv}_i}^{(n_t)}\Big)\right]^T,$$

$$\boldsymbol{\xi}_{\text{R-DN}} = \Big[\widetilde{\Delta f}_{\text{R-DN}}^{(1)}, \cdots, \widetilde{\Delta f}_{\text{R-DN}}^{(n_t)}\Big]^T,$$

$$\boldsymbol{\xi}_{\text{R-UP}} = \Big[\widetilde{\Delta f}_{\text{R-UP}}^{(1)}, \cdots, \widetilde{\Delta f}_{\text{R-UP}}^{(n_t)}\Big]^T$$

where $\boldsymbol{\beta}_{\text{p}_i}$, $\boldsymbol{\beta}_{\text{R-DN}_i}$ and $\boldsymbol{\beta}_{\text{R-UP}_i}$ are diagonal matrices $\in \mathbb{R}^{n_t \times n_t}$ with the $\beta_{\text{p}_i}^{(k)}$, $\beta_{\text{R-DN}_i}^{(k)}$ and $\beta_{\text{R-UP}_i}^{(k)}$ coefficients ($\forall k \in \mathcal{K}$) contained in their diagonal elements, respectively. When the frequency deviation is positive, the real time controller uses the reactive power policy (9a), whereas when the frequency deviation is negative, the real time controller uses the reactive power policy (9b). The two policies are equal when the frequency deviation is zero, or within the deadband

The active power policy that is responsible for charging

This article has been accepted for publication in a future issue of this journal, but has not been fully edited. Content may change prior to final publication. Citation information: DOI 10.1109/ACCESS.2020.3018086, IEEE Access

and discharging VC batteries can be defined as:

$$\tilde{\boldsymbol{P}}_{\text{VC, bat}_i} = \left[\tilde{p}^{(1)}_{\text{VC, bat}_i}, \cdots, \tilde{p}^{(n_t)}_{\text{VC, bat}_i}\right]^T = \boldsymbol{Z}_{\text{p}_i} \boldsymbol{\xi}_{\Delta p}, \forall i \in \mathcal{I} \tag{11}$$

where $\tilde{p}^{(k)}_{\text{VC, bat}_i}$ is the uncertain active power of the VC battery i at time step k. $\boldsymbol{Z}_{\text{p}_i}$ is a diagonal matrix $\in \mathbb{R}^{n_t \times n_t}$, with $z^{(k)}_{\text{p}_i}$ ($\forall k \in \mathcal{K}$) the coefficients of the active power policy contained in its diagonal elements.

For each time step k, the coefficients of the reactive and active power policies are calculated considering the following cases:

1) In the case the offline controller predicts a voltage rise problem:
   a) If VC batteries are predicted not to be charged, the offline controller sets $z^{(k)}_{\text{p}_i}$ to zero, and maximizes the upward-FCR capacity ($r^{(k)}_{\text{UP}_i}$) and downward-FCR capacity ($r^{(k)}_{\text{DN}_i}$) considering limits of batteries, inverters and voltages. $\beta^{(k)}_{\text{p}_i}$, $\beta^{(k)}_{\text{R-DN}_i}$ and $\beta^{(k)}_{\text{R-UP}_i}$ are calculated considering the following cases:
      i) Negative frequency deviation case (upward-FCR): $\beta^{(k)}_{\text{p}_i}$ is calculated to solve the voltage rise problem predicted to be caused by reverse power flow from PV units, whereas $\beta^{(k)}_{\text{R-UP}_i}$ is calculated to solve the voltage rise problem that may arise from discharging R-UP batteries.
      ii) Positive frequency deviation case (downward-FCR): $\beta^{(k)}_{\text{p}_i}$ is calculated to solve the voltage rise problem taking into account the effect of charging R-DN batteries on mitigating voltage rise. $\beta^{(k)}_{\text{R-DN}_i}$ is included in the calculation of reactive power to let the real time controller be aware that charging R-DN batteries helps in mitigating voltage rise problem and less reactive power is needed.
   b) If VC batteries are predicted to be charged:
      i) Negative frequency deviation case: the offline controller sets the upward-FCR capacity to zero, as it is impossible to charge and discharge the real battery at the same time. Logic constraints (presented in subsection V-G) are used to set the upward-FCR capacity at time step k and $\beta^{(k)}_{\text{R-UP}_i}$ to zero. $\beta^{(k)}_{\text{p}_i}$ is calculated to solve the predicted voltage rise problem considering the help from VC batteries ($z^{(k)}_{\text{p}_i} < 0$).
      ii) Positive frequency deviation case: the offline controller maximizes the downward-FCR capacity considering limits of batteries, inverters and voltages. $\beta^{(k)}_{\text{p}_i}$ and $z^{(k)}_{\text{p}_i}$ are calculated to solve the voltage rise problem taking into account the effect of charging the R-DN batteries on mitigating voltage rise (which is included in $\beta^{(k)}_{\text{R-DN}_i}$).
2) In the case the offline controller predicts a voltage drop problem: the same logic is applied.
3) In the case the offline controller predicts no voltage problem: the upward-FCR and downward-FCR capacities are maximized considering constraints related to batteries, inverters and voltages. The offline controller sets $\beta^{(k)}_{\text{p}_i}$ and $z^{(k)}_{\text{p}_i}$ to zero. $\beta^{(k)}_{\text{R-UP}_i}$ is calculated to avoid any voltage rise problem that may arise from discharging R-UP batteries, whereas $\beta^{(k)}_{\text{R-DN}_i}$ is calculated to avoid any voltage drop problem that may arise from charging R-DN batteries.

It is worth to point out that to reduce the measurements and communication overhead of the real time controller, the reactive and active power policies are designed as linear functions of only the households' active power consumption and PV power of control nodes. In real time, the control policies do not consider the households' active power consumption of passive nodes, but we do consider the effect of passive nodes' active power consumption on voltages in the branch flow model of the offline optimization, as will be shown in subsection V-F.

Energy Management Policies

In [23], a linear energy management policy to regulate the state of charge of a battery while providing FCR is presented. For each time step k, the power of this energy management policy is designed as a linear function of normalized frequency deviations that belong to the set $\left\{\widetilde{\Delta f}^{(1)}, \cdots, \widetilde{\Delta f}^{(k-1)}\right\}$. In this paper, we adapt this policy to be used for regulating the energy content of R-UP batteries and R-DN batteries. For each time step k, the power of the R-UP battery management policy $\tilde{p}^{(k)}_{\text{m-UP, bat}_i}$ is expressed as a linear function of negative frequency deviations that belong to the set $\left\{\widetilde{\Delta f}^{(1)}_{\text{R-UP}}, \cdots, \widetilde{\Delta f}^{(k-1)}_{\text{R-UP}}\right\}$, whereas power of the R-DN battery management policy $\tilde{p}^{(k)}_{\text{m-DN, bat}_i}$ is expressed as a linear function of positive frequency deviations that belong to the set $\left\{\widetilde{\Delta f}^{(1)}_{\text{R-DN}}, \cdots, \widetilde{\Delta f}^{(k-1)}_{\text{R-DN}}\right\}$:

$$\begin{aligned}
\tilde{p}^{(k)}_{\text{m-DN, bat}_i} &= \sum_{\varkappa=1}^{k-1} \left(m^{(\varkappa)}_{\text{R-DN}_i}\right)^{(k)} \widetilde{\Delta f}^{(\varkappa)}_{\text{R-DN}}, \forall i \in \mathcal{I}, \forall k \in \mathcal{K} \\
\tilde{\boldsymbol{P}}^{(k)}_{\text{m-DN, bat}_i} &= \left[\tilde{p}^{(1)}_{\text{m-DN, bat}_i}, \cdots, \tilde{p}^{(n_t)}_{\text{m-DN, bat}_i}\right]^T \\
&= \boldsymbol{M}_{\text{R-DN}_i} \boldsymbol{\xi}_{\text{R-DN}}, \forall i \in \mathcal{I}
\end{aligned} \tag{12}$$

with $\left(m^{(\varkappa)}_{\text{R-DN}_i}\right)^{(k)}$, $\varkappa = 1, \cdots, k-1$ ($\forall k \in \mathcal{K}$), the coefficients of the R-DN battery management policy i, contained in the lower triangular matrix $\boldsymbol{M}_{\text{R-DN}_i} \in \mathbb{R}^{n_t \times n_t}$ with zeros on the diagonal.

With $\left(m^{(\varkappa)}_{\text{R-UP}_i}\right)^{(k)}$, $\varkappa = 1, \cdots, k-1$ ($\forall k \in \mathcal{K}$), as

This article has been accepted for publication in a future issue of this journal, but has not been fully edited. Content may change prior to final publication. Citation information: DOI 10.1109/ACCESS.2020.3018086, IEEE Access

the coefficients of the R-UP battery management policy i, contained in the lower triangular matrix $\boldsymbol{M}_{\text{R-UP}_i} \in \mathbb{R}^{n_t \times n_t}$ with zeros on the diagonal, the power of the R-UP battery management policy $\tilde{p}^{(k)}_{\text{m-UP, bat}_i}$ ($\forall k \in \mathcal{K}$) can be defined as:

$$\begin{aligned}\tilde{\boldsymbol{P}}^{(k)}_{\text{m-UP, bat}_i} &= \left[\tilde{p}^{(1)}_{\text{m-UP, bat}_i}, \cdots, \tilde{p}^{(n_t)}_{\text{m-UP, bat}_i}\right]^T \\ &= \boldsymbol{M}_{\text{R-UP}_i}\boldsymbol{\xi}_{\text{R-UP}}, \forall i \in \mathcal{I} \end{aligned} \tag{13}$$

C. ALLOCATION OF BESS CAPACITY

As shown in Fig. 5, the offline controller allocates fractions of the energy and power capacity of each BESS to the voltage and frequency control services. For each time step k, the energy content of each battery is divided into three parts that provide upward-FCR, downward-FCR, and voltage control. The constraints (14a)-(14h) allocate the maximum, minimum, and initial energy capacity for each part:

$\forall k \in \mathcal{K}, \forall i \in \mathcal{I}$

Stochastic constraints:

$$\underline{e}^{(k)}_{\text{VC, bat}_i} \leqslant \tilde{E}^{(k)}_{\text{VC, bat}_i} \leqslant \overline{e}^{(k)}_{\text{VC, bat}_i} \tag{14a}$$

$$\underline{e}^{(k)}_{\text{R-UP, bat}_i} \leqslant \tilde{E}^{(k)}_{\text{R-UP, bat}_i} \leqslant \overline{e}^{(k)}_{\text{R-UP, bat}_i} \tag{14b}$$

$$\underline{e}^{(k)}_{\text{R-DN, bat}_i} \leqslant \tilde{E}^{(k)}_{\text{R-DN, bat}_i} \leqslant \overline{e}^{(k)}_{\text{R-DN, bat}_i} \tag{14c}$$

Other constraints:

$$\underline{e}^{(k)}_{\text{VC, bat}_i} \geq 0,\ \underline{e}^{(k)}_{\text{R-UP, bat}_i} \geq 0,\ \underline{e}^{(k)}_{\text{R-DN, bat}_i} \geq 0 \tag{14d}$$

$$\overline{e}^{(k)}_{\text{VC, bat}_i} \geq 0,\ \overline{e}^{(k)}_{\text{R-UP, bat}_i} \geq 0,\ \overline{e}^{(k)}_{\text{R-DN, bat}_i} \geq 0 \tag{14e}$$

$$\underline{e}^{(k)}_{\text{VC, bat}_i} + \underline{e}^{(k)}_{\text{R-UP, bat}_i} + \underline{e}^{(k)}_{\text{R-DN, bat}_i} \geq \underline{e}_{\text{bat}_i} \tag{14f}$$

$$\overline{e}^{(k)}_{\text{VC, bat}_i} + \overline{e}^{(k)}_{\text{R-UP, bat}_i} + \overline{e}^{(k)}_{\text{R-DN, bat}_i} \leq \overline{e}_{\text{bat}_i} \tag{14g}$$

$$E^0_{\text{VC, bat}_i} + E^0_{\text{R-UP, bat}_i} + E^0_{\text{R-DN, bat}_i} \leq E^0_{\text{bat}_i} \tag{14h}$$

Here, $\tilde{E}^{(k)}_{\text{VC, bat}_i}$, $\tilde{E}^{(k)}_{\text{R-UP, bat}_i}$ and $\tilde{E}^{(k)}_{\text{R-DN, bat}_i}$ are, respectively, the uncertain energy contents of the VC battery i, R-UP battery i, and R-DN battery i at time step k. The model of the uncertain energy contents of the virtual batteries is presented in subsection V-D. $\overline{e}_{\text{bat}_i}$ and $\underline{e}_{\text{bat}_i}$ denote, respectively, the maximum and minimum energy capacity of battery i. $\overline{e}^{(k)}_{\text{VC, bat}_i}$, $\overline{e}^{(k)}_{\text{R-UP, bat}_i}$ and $\overline{e}^{(k)}_{\text{R-DN, bat}_i}$ denote maximum energy capacities of the VC battery i, R-UP battery i, and R-DN battery i at time step k. $\underline{e}^{(k)}_{\text{VC, bat}_i}$, $\underline{e}^{(k)}_{\text{R-UP, bat}_i}$ and $\underline{e}^{(k)}_{\text{R-DN, bat}_i}$ denote minimum energy capacities of the VC battery i, R-UP battery i, and R-DN battery i at time step k. $E^0_{\text{bat}_i}$, $E^0_{\text{VC, bat}_i}$, $E^0_{\text{R-UP, bat}_i}$ and $E^0_{\text{R-DN, bat}_i}$ denote the initial energy contents of the battery i, VC battery i, R-UP battery i, and R-DN battery i, respectively.

To operate the control system sustainably, the energy contents of the BESSs at the end of the day need to be close to that of the start of the day. To this end, we define the following constraint to force the maximum energy at the end of the day to be less than or equal the initial energy content.

$$\overline{e}^{(n_t)}_{\text{VC, bat}_i} + \overline{e}^{(n_t)}_{\text{R-UP, bat}_i} + \overline{e}^{(n_t)}_{\text{R-DN, bat}_i} \leq E^0_{\text{bat}i} \tag{15}$$

For each time step k, the maximum charge power capacity

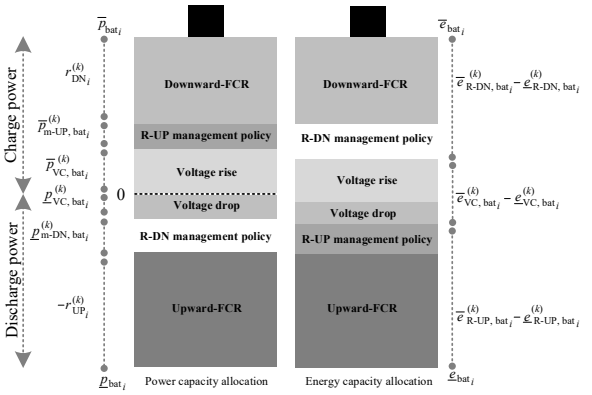

Fig. 5: Illustration of energy and power capacity allocation of battery i.

$\overline{p}_{\text{bat}_i}$ of battery i is divided into 3 parts: downward-FCR capacity $r^{(k)}_{\text{DN}_i}$; power capacity $\overline{p}^{(k)}_{\text{m-UP, bat}_i}$ of the R-UP battery management policy; and power capacity $\overline{p}^{(k)}_{\text{VC, bat}_i}$ of the voltage rise control. The maximum discharge power capacity (or minimum power capacity) of battery i $\underline{p}_{\text{bat}_i}$ is divided, for each time step k, into 3 parts: upward-FCR capacity $r^{(k)}_{\text{UP}_i}$; power capacity $\underline{p}^{(k)}_{\text{m-DN, bat}_i}$ of the R-DN battery management policy; and power capacity $\underline{p}^{(k)}_{\text{VC, bat}_i}$ of the voltage drop control. The constraints (16a)-(16f) allocate the power capacity for each part:

$\forall k \in \mathcal{K}, \forall i \in \mathcal{I}$

Stochastic constraints:

$$\underline{p}^{(k)}_{\text{VC, bat}_i} \leqslant \tilde{p}^{(k)}_{\text{VC, bat}_i} \leqslant \overline{p}^{(k)}_{\text{VC, bat}_i} \tag{16a}$$

$$0 \leqslant \tilde{p}^{(k)}_{\text{m-UP, bat}_i} \leqslant \overline{p}^{(k)}_{\text{m-UP, bat}_i} \tag{16b}$$

$$\underline{p}^{(k)}_{\text{m-DN, bat}_i} \leqslant \tilde{p}^{(k)}_{\text{m-DN, bat}_i} \leqslant 0 \tag{16c}$$

Other constraints:

$$r^{(k)}_{\text{UP}_i} \geq 0,\ r^{(k)}_{\text{DN}_i} \geq 0 \tag{16d}$$

$$\underline{p}^{(k)}_{\text{VC, bat}_i} - r^{(k)}_{\text{UP}_i} + \underline{p}^{(k)}_{\text{m-DN, bat}_i} \geq \underline{p}_{\text{bat}_i} \tag{16e}$$

$$\overline{p}^{(k)}_{\text{VC, bat}_i} + r^{(k)}_{\text{DN}_i} + \overline{p}^{(k)}_{\text{m-UP, bat}_i} \leq \overline{p}_{\text{bat}_i} \tag{16f}$$

The power of the R-UP management policy is defined as a charge power in (16b), to avoid discharging the R-UP battery to less than its minimum energy capacity while providing upward-FCR. The power of the R-DN management policy is defined as a discharge power in (16c), to avoid charging the R-DN battery to more than its maximum energy capacity while providing donward-FCR. In (16a), the power of the VC battery varies between negative power capacity $\underline{p}^{(k)}_{\text{VC, bat}_i}$ (discharge power), and positive power capacity $\overline{p}^{(k)}_{\text{VC, bat}_i}$ (charge power). The VC battery can be charged to reduce the reverse power flow from PV installations during PV peak period, which helps mitigate voltage rise. During load peak period, the VC battery can be discharged to feed a local load, which helps mitigate voltage drop.

This article has been accepted for publication in a future issue of this journal, but has not been fully edited. Content may change prior to final publication. Citation information: DOI 10.1109/ACCESS.2020.3018086, IEEE Access

D. BATTERY MODEL

We consider a simple discrete battery model for the three virtual batteries:

$$\tilde{E}^{(k+1)}_{\text{VC, bat}_i} = \tilde{E}^{(k)}_{\text{VC, bat}_i} + \Delta t\Bigg(\eta_i^{\text{ch}}\left[\tilde{p}^{(k)}_{\text{VC, bat}_i}\right]^+ - \frac{1}{\eta_i^{\text{dis}}}\left[-\tilde{p}^{(k)}_{\text{VC, bat}_i}\right]^+\Bigg) \tag{17a}$$

$$\tilde{E}^{(k+1)}_{\text{R-DN, bat}_i} = \tilde{E}^{(k)}_{\text{R-DN, bat}_i} + \Delta t\left(\eta_i^{\text{ch}}\tilde{p}^{(k)}_{\text{R-DN}_i} + \frac{1}{\eta_i^{\text{dis}}}\tilde{p}^{(k)}_{\text{m-DN, bat}_i}\right),$$

$$\tilde{p}^{(k)}_{\text{R-DN}_i} = r^{(k)}_{\text{DN}_i}\widetilde{\Delta f}^{(k)}_{\text{R-DN}} \tag{17b}$$

$$\tilde{E}^{(k+1)}_{\text{R-UP, bat}_i} = \tilde{E}^{(k)}_{\text{R-UP, bat}_i} + \Delta t\left(\eta_i^{\text{ch}}\tilde{p}^{(k)}_{\text{m-UP, bat}_i} + \frac{1}{\eta_i^{\text{dis}}}\tilde{p}^{(k)}_{\text{R-UP}_i}\right),$$

$$\tilde{p}^{(k)}_{\text{R-UP}_i} = r^{(k)}_{\text{UP}_i}\widetilde{\Delta f}^{(k)}_{\text{R-UP}} \tag{17c}$$

Here, η_i^{ch} and η_i^{dis} are, respectively, the charge and discharge efficiencies of battery i. $\tilde{p}^{(k)}_{\text{R-DN}_i}$ and $\tilde{p}^{(k)}_{\text{R-UP}_i}$ are, respectively, the uncertain downward-FCR power and upward-FCR power at time step k. In (17a), the operator $[\cdot]^+ \equiv \max(\cdot, 0)$ introduces integer variables to the stochastic constraint (14a), which results in a mixed integer stochastic constraint. As mixed integer stochastic constraints lead to a high computational complexity, a heuristic approach is proposed in [23] to get rid of integer variables of a battery model providing FCR. In this paper, we adapt the heuristic approach to be used for a battery model providing voltage control:

$$\tilde{E}^{(k+1)}_{\text{VC, bat}_i} = \tilde{E}^{(k)}_{\text{VC, bat}_i} + \Delta t\Bigg(\left[\left(\tilde{p}^{(k)}_{\text{VC, bat}_i}\right)_{\eta^{(k)}}\right]^+ - \left[-\left(\tilde{p}^{(k)}_{\text{VC, bat}_i}\right)_{\eta^{(k)}}\right]^+\Bigg), \tag{18}$$

$$\tilde{E}^{(k+1)}_{\text{VC, bat}_i} = \tilde{E}^{(k)}_{\text{VC, bat}_i} + \Delta t\left(\tilde{p}^{(k)}_{\text{VC, bat}_i}\right)_{\eta^{(k)}},$$

$$\left(\tilde{p}^{(k)}_{\text{VC, bat}_i}\right)_{\eta^{(k)}} = \begin{cases} \eta_i^{\text{ch}}\tilde{p}^{(k)}_{\text{VC, bat}_i} & \text{if } p^{(k)}_{l_i} \leqslant p^{(k)}_{\text{pv}_i} \\ \frac{1}{\eta_i^{\text{dis}}}\tilde{p}^{(k)}_{\text{VC, bat}_i} & \text{if } p^{(k)}_{l_i} > p^{(k)}_{\text{pv}_i} \end{cases}$$

The if condition in (18) is based on the fact that the controller tends to discharge the battery when the load is higher than the PV generation (to mitigate voltage drop) and charge the battery when the PV generation is higher than the load (to mitigate voltage rise). Our simulation results show that this heuristic approach does not lead to violation of the constraint (14a). In fact, (18) is the same as (17a) if $\text{sign}\left(p^{(k)}_{l_i,\text{meas}} - p^{(k)}_{\text{pv}_i,\text{meas}}\right) = -\text{sign}\left(p^{(k)}_{\text{bat}_i}\right)$, where $p^{(k)}_{l_i,\text{meas}}$ and $p^{(k)}_{\text{pv}_i,\text{meas}}$ are, respectively, the real time measured active power consumption and PV power generation at time step k.

Degradation Cost

The per-kWh battery degradation cost proposed in [34] is applied in this paper:

$$c_{\text{p}_i} = \frac{c_{\text{replacement}_i}}{N_{\text{cycle life}} \times \text{DoD} \times 2\overline{e}_{\text{bat}_i}} \tag{19}$$

Here, c_{p_i} is the battery degradation cost per kWh (cent/kWh), $c_{\text{replacement}_i}$ is the battery replacement cost, $N_{\text{cycle life}}$ is the battery cycle life, and DoD is the depth-of-discharge. The denominator of (19) gives the charging and discharging kWh the real battery can tolerate over its serviceable life.

E. INVERTER MODEL

The active and reactive power passing through inverter i is limited by its apparent power capacity:

$$\sqrt{(\tilde{p}^{(k)}_{\text{R-DN, inv}_i})^2 + (\tilde{q}^{(k)}_{\text{R-DN, inv}_i})^2} \leqslant \overline{s}_{\text{inv}_i}, \forall i \in \mathcal{I}, \forall k \in \mathcal{K},$$
$$\tilde{p}^{(k)}_{\text{R-DN, inv}_i} = -\tilde{p}^{(k)}_{\text{pv}_i} + \left(\tilde{p}^{(k)}_{\text{R-DN}_i}\right) + \tilde{p}^{(k)}_{\text{VC, bat}_i} + \tilde{p}^{(k)}_{\text{m-DN, bat}_i} + \tilde{p}^{(k)}_{\text{m-UP, bat}_i} \tag{20a}$$

$$\sqrt{(\tilde{p}^{(k)}_{\text{R-UP, inv}_i})^2 + (\tilde{q}^{(k)}_{\text{R-UP, inv}_i})^2} \leqslant \overline{s}_{\text{inv}_i}, \forall i \in \mathcal{I}, \forall k \in \mathcal{K},$$
$$\tilde{p}^{(k)}_{\text{R-UP, inv}_i} = -\tilde{p}^{(k)}_{\text{pv}_i} + \left(\tilde{p}^{(k)}_{\text{R-UP}_i}\right) + \tilde{p}^{(k)}_{\text{VC, bat}_i} + \tilde{p}^{(k)}_{\text{m-DN, bat}_i} + \tilde{p}^{(k)}_{\text{m-UP, bat}_i} \tag{20b}$$

The stochastic constraint (20a) considers the possibility of a positive frequency deviation case, whereas the stochastic constraint (20b) considers the possibility of a negative frequency deviation case. The two constraints are equal if the frequency deviation is zero, or within the deadband. $\overline{s}_{\text{inv}_i}$ is the maximum magnitude of apparent power of inverter i. $\tilde{p}^{(k)}_{\text{R-DN, inv}_i}$ is the uncertain active power of inverter i at time step k that considers the downward-FCR power, whereas $\tilde{p}^{(k)}_{\text{R-UP, inv}_i}$ is the uncertain active power of inverter i at time step k that considers the upward-FCR power. $\tilde{p}^{(k)}_{\text{R-DN}_i}$ and $\tilde{p}^{(k)}_{\text{R-UP}_i}$ cannot be included in one equation, as both $r^{(k)}_{\text{DN}_i}$ and $r^{(k)}_{\text{UP}_i}$ can be greater than zero, but only one of them is applied in real time. This is because the frequency deviation in real time can be either positive or negative.

As shown in [27], the conic stochastic constraints (20a) and (20b) can be approximated by a number of linear stochastic constraints $n_{\mathcal{S}}$ with a relative error of $1 - \cos(\pi/2n_{\mathcal{S}})$:

$$-\overline{s}_{\text{inv}_i} \leqslant \cos(\vartheta\phi)\tilde{p}^{(k)}_{\text{R-DN, inv}_i} + \sin(\vartheta\phi)\tilde{q}^{(k)}_{\text{R-DN, inv}_i} \leqslant \overline{s}_{\text{inv}_i},$$
$$-\overline{s}_{\text{inv}_i} \leqslant \cos(\vartheta\phi)\tilde{p}^{(k)}_{\text{R-UP, inv}_i} + \sin(\vartheta\phi)\tilde{q}^{(k)}_{\text{R-UP, inv}_i} \leqslant \overline{s}_{\text{inv}_i},$$
$$\phi = \frac{\pi}{n_{\mathcal{S}}}, \ \vartheta = 1, \cdots, n_{\mathcal{S}} \tag{21}$$

Reactive Power Cost

The reactive power cost c_{q_i} (cent/kvarh), considered in this paper, corresponds to the approximative compensation cost of the additional inverter losses due to the reactive power utilization and is provided by [35].

F. BRANCH FLOW MODEL

In this paper, a linear branch flow model is applied. The model is based on the DistFlow method developed in [36]. According to [37], the linearized branch flow model tends

to introduce a small relative error of 1-5% when used for calculating power flows of real distribution networks.

$\forall k \in \mathcal{K}:$

$$(\tilde{\boldsymbol{v}}^{(k)})^2_{\text{R-DN}} = \boldsymbol{R}\tilde{\boldsymbol{P}}^{(k)}_{\text{I}} + \boldsymbol{X}\tilde{\boldsymbol{Q}}^{(k)}_{\text{I}} + v_o^2 \mathbf{1}_{n_{\text{nodes}}} \tag{22a}$$
$$\tilde{\boldsymbol{P}}^{(k)}_{\text{I}} = \left[\tilde{\boldsymbol{P}}^{(k)}_{\text{R-DN, node}}; \tilde{\boldsymbol{P}}^{(k)}_{\text{passive}}\right], \tilde{\boldsymbol{Q}}^{(k)}_{\text{I}} = \left[\tilde{\boldsymbol{Q}}^{(k)}_{\text{R-DN, node}}; \tilde{\boldsymbol{Q}}^{(k)}_{\text{passive}}\right]$$

$$(\tilde{\boldsymbol{v}}^{(k)})^2_{\text{R-UP}} = \boldsymbol{R}\tilde{\boldsymbol{P}}^{(k)}_{\text{II}} + \boldsymbol{X}\tilde{\boldsymbol{Q}}^{(k)}_{\text{II}} + v_o^2 \mathbf{1}_{n_{\text{nodes}}} \tag{22b}$$
$$\tilde{\boldsymbol{P}}^{(k)}_{\text{II}} = \left[\tilde{\boldsymbol{P}}^{(k)}_{\text{R-UP, node}}; \tilde{\boldsymbol{P}}^{(k)}_{\text{passive}}\right], \tilde{\boldsymbol{Q}}^{(k)}_{\text{II}} = \left[\tilde{\boldsymbol{Q}}^{(k)}_{\text{R-UP, node}}; \tilde{\boldsymbol{Q}}^{(k)}_{\text{passive}}\right]$$

Here, v_o is the substation voltage, which is considered constant. $\mathbf{1}_{n_{\text{nodes}}} \in \mathbb{R}^{n_{\text{nodes}}}$ is a vector of all ones. $(\tilde{\boldsymbol{v}}^{(k)})^2_{\text{R-DN}} = \left[(\tilde{v}_1^{(k)})^2_{\text{R-DN}}, \cdots, (\tilde{v}_{n_{\text{nodes}}}^{(k)})^2_{\text{R-DN}}\right]^T$ and $(\tilde{\boldsymbol{v}}^{(k)})^2_{\text{R-UP}} = \left[(\tilde{v}_1^{(k)})^2_{\text{R-UP}}, \cdots, (\tilde{v}_{n_{\text{nodes}}}^{(k)})^2_{\text{R-UP}}\right]^T$ denote vectors of squared nodal voltage magnitudes at time step k. The effect of charging R-DN batteries on voltage profiles is included in $(\tilde{\boldsymbol{v}}^{(k)})^2_{\text{R-DN}}$, whereas the effect of discharging R-UP batteries on voltage profiles is included in $(\tilde{\boldsymbol{v}}^{(k)})^2_{\text{R-UP}}$. The two effects cannot be included in one equation, as only one of them occurs in real time, but in the offline computation, both of them can be non-zero at time step k. For each time step, we consider the two effects in the offline optimization, to prepare the real time controller for the two cases: positive frequency deviation; and negative frequency deviation. The vectors $\tilde{\boldsymbol{P}}^{(k)}_{\text{R-DN, node}} = \left[\tilde{p}^{(k)}_{\text{R-DN, node}_1}, \cdots, \tilde{p}^{(k)}_{\text{R-DN, node}_{n_c}}\right]^T$ and $\tilde{\boldsymbol{P}}^{(k)}_{\text{R-UP, node}} = \left[\tilde{p}^{(k)}_{\text{R-UP, node}_1}, \cdots, \tilde{p}^{(k)}_{\text{R-UP, node}_{n_c}}\right]^T$ denote active powers of control nodes (at time step k) that consider, respectively, the downward-FCR power and upward-FCR power. The vectors $\tilde{\boldsymbol{Q}}^{(k)}_{\text{R-DN, node}} = \left[\tilde{q}^{(k)}_{\text{R-DN, node}_1}, \cdots, \tilde{q}^{(k)}_{\text{R-DN, node}_{n_c}}\right]^T$ and $\tilde{\boldsymbol{Q}}^{(k)}_{\text{R-UP, node}} = \left[\tilde{q}^{(k)}_{\text{R-UP, node}_1}, \cdots, \tilde{q}^{(k)}_{\text{R-UP, node}_{n_c}}\right]^T$ denote reactive powers of control nodes (at time step k) that consider, respectively, the downward-FCR power and upward-FCR power. The vectors $\tilde{\boldsymbol{P}}^{(k)}_{\text{passive}} = \left[\tilde{p}^{(k)}_{\text{passive}_{n_c+1}}, \cdots, \tilde{p}^{(k)}_{\text{passive}_{n_{\text{nodes}}}}\right]^T$ and $\tilde{\boldsymbol{Q}}^{(k)}_{\text{passive}} = \left[\tilde{q}^{(k)}_{\text{passive}_{n_c+1}}, \cdots, \tilde{q}^{(k)}_{\text{passive}_{n_{\text{nodes}}}}\right]^T$ include, respectively, active powers and reactive powers of passive nodes at time step k. If i is a control node and j is a passive node, then their active and reactive powers can be defined as:

$$\left.\begin{aligned}
\tilde{p}^{(k)}_{\text{R-DN, node}_i} &= \tilde{p}^{(k)}_{l_i} + \tilde{p}^{(k)}_{\text{R-DN, inv}_i} \\
\tilde{q}^{(k)}_{\text{R-DN, node}_i} &= \tilde{q}^{(k)}_{l_i} + \tilde{q}^{(k)}_{\text{R-DN, inv}_i} \\
\tilde{p}^{(k)}_{\text{R-UP, node}_i} &= \tilde{p}^{(k)}_{l_i} + \tilde{p}^{(k)}_{\text{R-UP, inv}_i} \\
\tilde{q}^{(k)}_{\text{R-UP, node}_i} &= \tilde{q}^{(k)}_{l_i} + \tilde{q}^{(k)}_{\text{R-UP, inv}_i}
\end{aligned}\right\} \forall i \in \mathcal{I} \tag{23}$$

$$\left.\begin{aligned}
\tilde{p}^{(k)}_{\text{passive}_j} &= \tilde{p}^{(k)}_{l_j} \\
\tilde{q}^{(k)}_{\text{passive}_j} &= \tilde{q}^{(k)}_{l_j}
\end{aligned}\right\} \forall j \in \mathcal{J} \tag{24}$$

The matrices $\boldsymbol{R}$ and $\boldsymbol{X}$ ($\in \mathbb{R}^{n_{\text{nodes}} \times n_{\text{nodes}}}$) depend, respectively, on the resistance and reactance of the network's feeders. We ask the readers to refer to [28] for details about the derivation of the above linearized branch flow model, and the computation of the matrices $\boldsymbol{R}$ and $\boldsymbol{X}$.

To maintain nodal voltage magnitudes within the maximum voltage limit $\overline{v}$ and the minimum voltage limit $\underline{v}$, we consider the following stochastic constraints:

$$\underline{v}^2 \leqslant (\tilde{\boldsymbol{v}}^{(k)})^2_{\text{R-DN}} \leqslant \overline{v}^2, \forall k \in \mathcal{K} \tag{25a}$$
$$\underline{v}^2 \leqslant (\tilde{\boldsymbol{v}}^{(k)})^2_{\text{R-UP}} \leqslant \overline{v}^2, \forall k \in \mathcal{K} \tag{25b}$$

G. LOGIC CONSTRAINTS

As has been discussed in subsection V-B, in the case VC batteries are predicted to be charged at time step k (to help in solving voltage rise problems), the offline controller sets $r^{(k)}_{\text{UP}_i}$ and $\beta^{(k)}_{\text{R-UP}_i}$ to zero. In the case VC batteries are expected to be discharged at time step k (to help in solving voltage drop problems), the offline controller sets $r^{(k)}_{\text{DN}_i}$ and $\beta^{(k)}_{\text{R-DN}_i}$ to zero. The following constraints are used to implement the aforementioned settings:

$$\text{If } \left(\overline{p}^{(k)}_{\text{VC, bat}_i} > 0 \text{ and } \underline{p}^{(k)}_{\text{VC, bat}_i} = 0\right), \tag{26a}$$
$$\text{then } r^{(k)}_{\text{UP}_i} = 0 \text{ and } \beta^{(k)}_{\text{R-UP}_i} = 0$$
$$\text{If } \left(\overline{p}^{(k)}_{\text{VC, bat}_i} = 0 \text{ and } \underline{p}^{(k)}_{\text{VC, bat}_i} < 0\right), \tag{26b}$$
$$\text{then } r^{(k)}_{\text{DN}_i} = 0 \text{ and } \beta^{(k)}_{\text{R-DN}_i} = 0$$

The solver used in the case study (YALMIP) transforms the above logic constraints into mixed integer linear constraints using Big-M strategy [38].

H. OBJECTIVE FUNCTION

The objective function of the proposed optimization problem aims at minimizing the expected cost of operating the voltage control system, and maximizing profits from FCR. The expected cost of operating the voltage control system is the sum of two costs: expected cost of the reactive power compensation; and batteries degradation cost. This results in the following objective function:

$$\begin{aligned}
\min \quad \mathbf{E}\Bigg[\sum_{i\in\mathcal{I}} c^2_{\text{q}_i} \Delta t^2 \Bigg(& \underbrace{\left\|\boldsymbol{\beta}_{\text{p}_i} \boldsymbol{\xi}_{\Delta p}\right\|^2_2}_{1} + \underbrace{\left\|\boldsymbol{\beta}_{\text{R-DN}_i} \boldsymbol{\xi}_{\text{R-DN}}\right\|^2_2}_{2} + \\
& \underbrace{\left\|\boldsymbol{\beta}_{\text{R-UP}_i} \boldsymbol{\xi}_{\text{R-UP}}\right\|^2_2}_{3} \Bigg) + c^2_{\text{p}_i} \Delta t^2 \Bigg(\underbrace{\left\|\boldsymbol{Z}_{\text{p}_i} \boldsymbol{\xi}_{\Delta p}\right\|^2_2}_{4} + \\
& \underbrace{\left\| \left(\boldsymbol{M}_{\text{R-DN}_i} + I_{\boldsymbol{R}_{\text{DN}_i}}\right) \boldsymbol{\xi}_{\text{R-DN}}\right\|^2_2}_{5} + \\
& \underbrace{\left\| \left(\boldsymbol{M}_{\text{R-UP}_i} + I_{\boldsymbol{R}_{\text{UP}_i}}\right) \boldsymbol{\xi}_{\text{R-UP}}\right\|^2_2}_{6} \Bigg) \Bigg] - \underbrace{\sum_{i\in\mathcal{I}} \left(\boldsymbol{R}_{\text{UP}_i} + \boldsymbol{R}_{\text{DN}_i}\right)}_{7}
\end{aligned} \tag{27}$$

Here, $\mathbf{E}[\cdot]$ denotes the expected value operator, and $\|\cdot\|_2$ is the second norm. Parts 1, 2 and 3 of the objective func-

This article has been accepted for publication in a future issue of this journal, but has not been fully edited. Content may change prior to final publication. Citation information: DOI 10.1109/ACCESS.2020.3018086, IEEE Access

tion represent sum of quadratic uncertain reactive powers of inverter i for n_t time steps. Uncertain reactive powers of parts 1, 2 and 3 are responsible for solving voltage problems expected to be caused by the reverse power flow from PV units, charging R-DN batteries, and discharging R-UP batteries, respectively. Parts 4, 5 and 6 of the objective function represent sum of quadratic uncertain active powers of battery i for n_t time steps. Uncertain active powers of part 4 are the uncertain charging and discharging powers of the VC battery i. Uncertain active powers of part 5 represent the uncertain charging powers of the downward-FCR and uncertain discharging powers of the R-DN management policy. Uncertain active powers of part 6 represent uncertain discharging powers of the upward-FCR and uncertain charging powers of the R-UP management policy. $I_{\boldsymbol{R}_{\mathrm{DN}_i}}$ in part 5 denotes a diagonal matrix $\in \mathbb{R}^{n_t \times n_t}$ with the vector of downward reserve capacities $\boldsymbol{R}_{\mathrm{DN}_i} = \left[r_{\mathrm{DN}_i}^{(1)}, \cdots, r_{\mathrm{DN}_i}^{(n_t)}\right]^T$ contained in its diagonal elements. $I_{\boldsymbol{R}_{\mathrm{UP}_i}}$ in part 6 denotes a diagonal matrix $\in \mathbb{R}^{n_t \times n_t}$ with the vector of upward reserve capacities $\boldsymbol{R}_{\mathrm{UP}_i} = \left[r_{\mathrm{UP}_i}^{(1)}, \cdots, r_{\mathrm{UP}_i}^{(n_t)}\right]^T$ contained in its diagonal elements. Part 7 is included in the objective function to maximize the upward and downward reserve capacities.

It can be shown that the objective function (27) can be written as:

$$\min \quad \mathbf{E}\left[\|F\boldsymbol{\zeta}\|_2^2\right] - \sum_{i\in\mathcal{I}}\left(\boldsymbol{R}_{\mathrm{UP}_i} + \boldsymbol{R}_{\mathrm{DN}_i}\right) \tag{28}$$

where $F \in \mathbb{R}^{6n_c n_t \times n_\zeta}$ can be defined to represent the first six parts of the objective function. A closed-form of the expected value in (28) is not readily available. A second-order moment matrix can be used to approximate the expected value, as discussed in [39]. If $\boldsymbol{M} = \mathbf{E}\left[\boldsymbol{\zeta}\boldsymbol{\zeta}^T\right]$ is a second-order moment matrix of the random vector $\boldsymbol{\zeta}$, then:

$$\mathbf{E}\left[\|F\boldsymbol{\zeta}\|_2^2\right] = \mathbf{E}\left[\mathrm{Tr}\left(F^T F\boldsymbol{\zeta}\boldsymbol{\zeta}^T\right)\right] = \mathrm{Tr}\left(F^T F\boldsymbol{M}\right) \tag{29}$$

where $\boldsymbol{M} \in \mathbb{R}^{n_\zeta \times n_\zeta}$ is assumed to be positive definite, and can be computed based on the following formula:

$$\boldsymbol{M} = \boldsymbol{\mu}_\zeta^T \boldsymbol{\mu}_\zeta + \mathrm{cov}\left(\boldsymbol{\zeta}^{\mathrm{scen}}\right) \tag{30}$$

Here, the matrix $\boldsymbol{\zeta}^{\mathrm{scen}} \in \mathbb{R}^{n_{\mathrm{scen}} \times n_\zeta}$ contains n_{scen} scenarios of the random vector $\boldsymbol{\zeta}$. $\boldsymbol{\mu} \in \mathbb{R}^{1 \times n_\zeta}$ is the sample mean of $\boldsymbol{\zeta}^{\mathrm{scen}}$, and $\mathrm{cov}\left(\boldsymbol{\zeta}^{\mathrm{scen}}\right)$ is the covariance matrix of $\boldsymbol{\zeta}^{\mathrm{scen}}$.

I. ROBUST OPTIMIZATION

Based on the previous linear models, one can show that the stochastic constraints (14a)-(14c), (16a)-(16c), (21), (25a), and (25b) can be written as:

$$\begin{aligned} &\boldsymbol{A}\boldsymbol{\zeta} \leq \boldsymbol{B}, \\ &\boldsymbol{A} \in \mathbb{R}^{(2n_c n_t(6+2n_s)+4n_{\mathrm{nodes}}n_t)\times n_\zeta}, \\ &\boldsymbol{B} \in \mathbb{R}^{(2n_c n_t(6+2n_s)+4n_{\mathrm{nodes}}n_t)} \end{aligned} \tag{31}$$

where the matrices $\boldsymbol{A}$ and $\boldsymbol{B}$ can be defined to represent the stochastic constraints mentioned above. To find a solution that remains feasible for any realization of $\boldsymbol{\zeta}$ in the uncertainty set $\mathcal{U}$, we consider the following robust counterpart of the stochastic constraint (31):

$$\max_{\boldsymbol{\zeta}\in\mathcal{U}} \boldsymbol{A}\boldsymbol{\zeta} \leqslant \boldsymbol{B} \tag{32}$$

Using standard duality techniques, it can be shown that the constraint (32) with a polyhedral uncertainty set $\mathcal{U}$ can be reformulated as the linear constraints (33b)-(33d). We ask the readers to refer to lemma 2 in [40] for details about robust counterpart of linear constraints with polyhedral uncertainty set. Below is the complete optimization problem the offline controller solves on a day-ahead basis:

$$\min \quad \mathrm{Tr}\left(F^T F\boldsymbol{M}\right) - \sum_{i\in\mathcal{I}}\left(\boldsymbol{R}_{\mathrm{UP}_i} + \boldsymbol{R}_{\mathrm{DN}_i}\right) \tag{33a}$$

subject to:

Robust constraints :

$$\boldsymbol{\pi}\boldsymbol{h} \leq \boldsymbol{B} \tag{33b}$$

$$\boldsymbol{\pi}\boldsymbol{H} \geq \boldsymbol{A} \tag{33c}$$

$$\boldsymbol{\pi} \geq 0 \tag{33d}$$

Logic constraints: (26a) and (26b) (33e)

Other constraints: (14d)-(14h), (15), (16d)-(16f) (33f)

The elements of the matrix $\boldsymbol{\pi} \in \mathbb{R}^{(2n_c n_t(6+2n_s)+4n_{\mathrm{nodes}}n_t)\times 2n_\zeta}$ are auxiliary variables.

The proposed optimization problem (33a)-(33f) is sensitive to the parameters of the uncertainty model $\mathcal{U}$ in (7), elements of the matrix $\boldsymbol{H}$ and the vector $\boldsymbol{h}$. Inappropriate setting of these parameters could lead to a more conservative solution or infeasible one. Hence, attention has to be paid to the settings of the uncertainty model. One can test the setting of the uncertainty model by running a numerical experiment over many scenarios; tuning can then be applied if necessary.

J. OPTIMALITY GAP

In this subsection, we investigate the loss of optimality of the robust optimization problem due to the use of linear control policies.

Robust optimization involving adaptive decision rules (control policies) is generally computationally intractable. To reduce its complexity, in subsection V-B we restrict the decision variables to be linear function of the uncertain data. In [39], an efficient method is proposed to estimate the approximation error introduced by this rather drastic means of complexity reduction. We apply the technique presented in [39] to estimate the optimality gap of the proposed robust optimization problem (33a)-(33f).

To compute the optimality gap, one needs to compute a lower and upper bounds on the optimal solution. The robust optimization problem (33a)-(33f) provides an upper bound (i.e., a conservative approximation) on the optimal solution, since it is formulated by reducing the underlying feasible set. The duality theorem can be used to obtain a lower bound on

This article has been accepted for publication in a future issue of this journal, but has not been fully edited. Content may change prior to final publication. Citation information: DOI 10.1109/ACCESS.2020.3018086, IEEE Access

the optimal solution. The dual problem of the problem

$$\min \quad \mathrm{Tr}\left(F^T F \boldsymbol{M}\right) - \sum_{i\in\mathcal{I}} \left(\boldsymbol{R}_{\mathrm{UP}_i} + \boldsymbol{R}_{\mathrm{DN}_i}\right) \tag{34a}$$

subject to:

$$\acute{\boldsymbol{A}}\boldsymbol{\zeta} + \boldsymbol{\Theta}\left(\boldsymbol{\zeta}\right) = 0 \tag{34b}$$

$$\text{Logic constraints: (26a) and (26b)} \tag{34c}$$

$$\text{Other constraints: (14d)-(14h), (15), (16d)-(16f)} \tag{34d}$$

can be derived as follows:

$$\min \max_{\boldsymbol{\lambda}\geq 0} \ \mathrm{Tr}\left(F^T F \boldsymbol{M}\right) - \sum_{i\in\mathcal{I}} \left(\boldsymbol{R}_{\mathrm{UP}_i} + \boldsymbol{R}_{\mathrm{DN}_i}\right) + \mathbf{E}\left[\boldsymbol{\lambda}\left(\boldsymbol{\zeta}\right)^T \left(\acute{\boldsymbol{A}}\boldsymbol{\zeta} + \boldsymbol{\Theta}\left(\boldsymbol{\zeta}\right)\right)\right] \tag{35a}$$

subject to:

$$\boldsymbol{\Theta}\left(\boldsymbol{\zeta}\right) \geq 0 \tag{35b}$$

$$\text{Logic constraints: (26a) and (26b)} \tag{35c}$$

$$\text{Other constraints: (14d)-(14h), (15), (16d)-(16f)} \tag{35d}$$

where $\acute{\boldsymbol{A}}\boldsymbol{\zeta} = \boldsymbol{A}\boldsymbol{\zeta} - \boldsymbol{B}$. The elements of the vector $\boldsymbol{\Theta}\left(\boldsymbol{\zeta}\right)$ are auxiliary variables, and $\boldsymbol{\lambda}\left(\boldsymbol{\zeta}\right)$ is a vector of dual decisions. The dual feasible set of the problem (35a)-(35d) can be restricted to combine only linear dual decisions. To this end, we require the dual decisions to be representable as $\boldsymbol{\lambda}\left(\boldsymbol{\zeta}\right) = \boldsymbol{\Lambda}\boldsymbol{\zeta}$. Based on this, the objective function (35a) can be reformulated as:

$$\min \max_{\boldsymbol{\Lambda}\geq 0} \ \mathrm{Tr}\left(F^T F \boldsymbol{M}\right) - \sum_{i\in\mathcal{I}} \left(\boldsymbol{R}_{\mathrm{UP}_i} + \boldsymbol{R}_{\mathrm{DN}_i}\right) + \mathbf{E}\left[\boldsymbol{\zeta}^T \boldsymbol{\Lambda}^T \left(\acute{\boldsymbol{A}}\boldsymbol{\zeta} + \boldsymbol{\Theta}\left(\boldsymbol{\zeta}\right)\right)\right] \tag{36a}$$

$$= \min \max_{\boldsymbol{\Lambda}\geq 0} \ \mathrm{Tr}\left(F^T F \boldsymbol{M}\right) - \sum_{i\in\mathcal{I}} \left(\boldsymbol{R}_{\mathrm{UP}_i} + \boldsymbol{R}_{\mathrm{DN}_i}\right) + \mathrm{Tr}\left(\boldsymbol{\Lambda}^T \mathbf{E}\left[\left(\acute{\boldsymbol{A}}\boldsymbol{\zeta} + \boldsymbol{\Theta}\left(\boldsymbol{\zeta}\right)\right)\boldsymbol{\zeta}^T\right]\right) \tag{36b}$$

The maximization in (36b) can be carried out explicitly. This yields to the following approximate problem.

$$\min \ \mathrm{Tr}\left(F^T F \boldsymbol{M}\right) - \sum_{i\in\mathcal{I}} \left(\boldsymbol{R}_{\mathrm{UP}_i} + \boldsymbol{R}_{\mathrm{DN}_i}\right) \tag{37a}$$

subject to:

$$\mathbf{E}\left[\left(\acute{\boldsymbol{A}}\boldsymbol{\zeta} + \boldsymbol{\Theta}\left(\boldsymbol{\zeta}\right)\right)\boldsymbol{\zeta}^T\right] = 0 \tag{37b}$$

$$\boldsymbol{\Theta}\left(\boldsymbol{\zeta}\right) \geq 0 \tag{37c}$$

$$\text{Logic constraints: (26a) and (26b)} \tag{37d}$$

$$\text{Other constraints: (14d)-(14h), (15), (16d)-(16f)} \tag{37e}$$

It is proved in [39] that the problem (37a)-(37e) provides a lower bound on the optimal solution. It can be shown that a tractable reformulation of this problem can be given as follows:

$$\min \ \mathrm{Tr}\left(F^T F \boldsymbol{M}\right) - \sum_{i\in\mathcal{I}} \left(\boldsymbol{R}_{\mathrm{UP}_i} + \boldsymbol{R}_{\mathrm{DN}_i}\right) \tag{38a}$$

subject to:

$$\acute{\boldsymbol{A}} + \boldsymbol{\theta} = 0 \tag{38b}$$

$$\left(\boldsymbol{H} - \boldsymbol{h}\boldsymbol{o}_1^T\right)\boldsymbol{M}\boldsymbol{\theta}^T \leq 0 \tag{38c}$$

$$\text{Logic constraints: (26a) and (26b)} \tag{38d}$$

$$\text{Other constraints: (14d)-(14h), (15), (16d)-(16f)} \tag{38e}$$

Here, $\boldsymbol{o}_1$ denotes a vector whose first element is 1 while all the others are 0. The matrix $\boldsymbol{H}$ and the vector $\boldsymbol{h}$ are defined in subsection V-A to model the uncertainty set $\mathcal{U}$. The second-order moment matrix $\boldsymbol{M}$ defined in subsection V-H is used to approximate the expected value in (37b). This approximation should respect the constraint (38c). The elements of the matrix $\boldsymbol{\theta}$ are auxiliary variables that respect the following relation:

$$\boldsymbol{\theta}\boldsymbol{M} = \mathbf{E}\left[\boldsymbol{\Theta}\left(\boldsymbol{\zeta}\right)\boldsymbol{\zeta}^T\right] \tag{39}$$

The optimality gap can be computed by comparing the solution of the problem (33a)-(33f) (upper bound) to the solution of the problem (38a)-(38e) (lower bound). We ask the reader to refer to [39] for an in-depth analysis of the sub-optimality of robust optimization with linear decision rules.

VI. CASE STUDY

A. SIMULATED NETWORK

We demonstrate the robust performance of the proposed control system on a low voltage 120-bus network (Fig. 6). This three-phase semi-urban radial distribution network operates with a nominal voltage of 230/400 V. All main feeder cables are of type EAXVB 1 kV 4×150 mm^2 (impedance: 0.206+j0.0778 Ω/km), except for the cable between node I and node II, which is of type EAXVB 1 kV 4×95 mm^2 (impedance: 0.320+j0.0778 Ω/km). The cables connecting each household with the feeder are of type EXVB-Cu 1 kV 4×16 mm^2, with a fixed length of 30 m (impedance: 1.15+j0.0828 Ω/km). The length of the cables II-III, II-IV, IV-V and IV-VI is 100 m; the length of the cables IV-X and VIII-IX is 200 m; the length of the cable IV-VII is 80 m.

The numbered nodes in the network are control nodes ($n_c = 60$) and the other nodes are passive nodes. The households' loads, inverters and batteries between II and III in Fig. 6 belong to group G1, between II and IV belong to group G2, between IV and V belong to group G3, between IV and VI belong to group G3, between IV and VII belong to group G4, between VIII and IX belong to group G4, and between VIII and X belong to group G5. The parameters of each group are listed in Table 1.

To comply with the European standard EN 50160 on power quality [41], the voltage limits $\overline{v}$ and $\underline{v}$ are enforced to be 10% of the nominal phase voltage 230 V, resulting in $\overline{v}$= 253 V and $\underline{v}$ = 207 V. The number of linear constraints n_s used to approximate the conic constraints (20a) and (20b) is set to 5.

B. THE LOADS, PV AND FREQUENCY SCENARIOS

For a weekday in June, we generate 10^4 daily profiles of households' active power consumption and PV power gener-

This article has been accepted for publication in a future issue of this journal, but has not been fully edited. Content may change prior to final publication. Citation information: DOI 10.1109/ACCESS.2020.3018086, IEEE Access

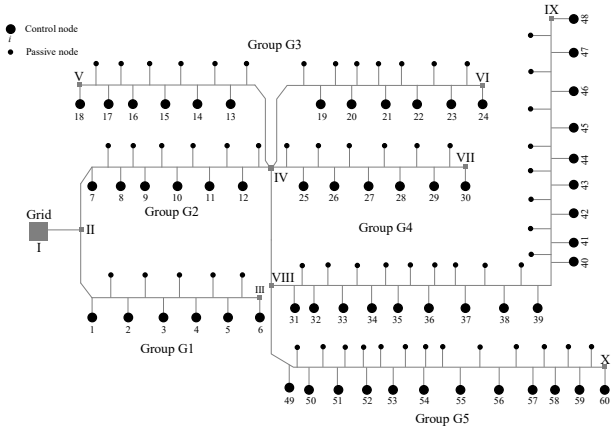

Fig. 6: Schematic diagram of the network used in this case study.

TABLE 1: Parameters of inverters, batteries and loads

	G1	G2	G3	G4	G5
$\overline{s}_{\text{inv}}$ (kVA)	5	8	10	12	15
$\overline{e}_{\text{bat}}$ (kWh)	4.8	7.2	8.2	9.8	13.5
$\underline{e}_{\text{bat}}$ (kWh)	0.96	1.44	1.64	1.96	2.7
E^{0}_{bat} (kWh)	2.4	3.6	4.1	4.9	6.75
$\overline{p}_{\text{bat}}$ (kW)	2	3	3.3	5	7
$\underline{p}_{\text{bat}}$ (kW)	-2	-3	-3.3	-5	-7
$N_{\text{cycle life}}$	3500	3500	3500	5000	5000
DoD (%)	80	80	80	80	80
$c_{\text{replacement}_i}$ (€)	2400	3600	4100	4900	6750
c_{p} (cent/kWh)	8.92	8.92	8.92	6.25	6.25
c_{q} (cent/kvarh)	0.29	0.29	0.29	0.29	0.29
η_i^{ch}	$\sqrt{0.9}$	$\sqrt{0.9}$	$\sqrt{0.9}$	$\sqrt{0.9}$	$\sqrt{0.9}$
η_i^{dis}	$\sqrt{0.9}$	$\sqrt{0.9}$	$\sqrt{0.9}$	$\sqrt{0.9}$	$\sqrt{0.9}$
Load kW-peak	3.5	5.6	7	8.4	10.5
Power factor	0.85	0.85	0.85	0.85	0.85
PV kW-peak	4.8	7.68	9.6	11.52	13.44

ation, with one-minute resolution. We consider the mean of the daily profiles as the forecasted households' active power consumption and PV power generation, and the maximum of the generated profiles as the maximum uncertain households' active power consumption and PV power generation. An open-source CREST DEMAND MODEL [42] is used in this paper to generate the households' active power consumption profiles. The daily PV profiles are generated based on the model presented in [43]. We use locally measured frequency data in the CE synchronous region with a resolution of 1 minute over a period of four years (2015-2018), to generate 10^4 daily frequency profiles.

C. SIMULATION SOFTWARE

The robust optimization problem (33a)-(33f) is solved using YALMIP [44] toolbox with Mosek 9.0 [45]. The MATPOWER package 7.0 [46] for power flow analysis is used to compute voltage profiles of network's nodes with and without the proposed control system. 15-minute time step resolution is considered in Yalmip simulations. To have daily profiles with 15-minute resolution, we take the average over 15 minutes for each one-minute resolution profile. One-minute time step resolution is considered in MATPOWER simulations, therefore, one active control policy, one reactive control policy, one R-DN energy management policy, and one R-UP energy management policy are considered for each 15 minutes simulation in MATPOWER. We select 5000 daily profiles (of loads, PV and frequency) randomly as training data (offline computation). All the generated profiles are considered in the validation (MATPOWER simulations).

D. SIMULATION RESULTS

Fig. 7 shows aggregated power capacities of the 60 BESSs reserved for the downward-FCR, upward-FCR, voltage rise, voltage drop, energy management policies of R-DN and R-UP batteries. The upward reserve capacity is defined as a positive value in (16d); it is presented as a negative power in Fig. 7 to compare it to the maximum discharging power. One can notice that the upward reserve capacity is zero from 10:00 till 14:30, this is because VC batteries are expected to be charged over this period. The downward reserve capacity is zero between 20:00 and 24:00, this is because batteries are expected to be discharged over this period to reach an energy content at the end of the day close to that of the start of the day, and to solve the voltage drop problem. The negative power capacity between 20:00 and 24:00 represents the power capacity reserved for discharging the VC batteries and the R-UP batteries. The highlighted positive power area between 10:00 and 14:30 shows the aggregated power capacity reserved for solving voltage rise problems. The aggregated downward reserve capacity is at minimum at 10:45, since most of the inverters capacity is occupied by the PV power, VC batteries power, and reactive power. The highlighted negative power area in Fig. 7 shows the aggregated power capacity reserved for the management policy of R-DN batteries. There is no power capacity reserved for the management policy of R-DN batteries between 20:00 and 24:00. The highlighted positive area between 00:00 and 10:00 and between 14:30 and 24:00 shows the aggregated power capacity reserved for the management policy of R-UP batteries. There is no power capacity reserved for the management policy of R-UP batteries between 10:00 and 14:30.

Fig. 8 shows the power capacity reserved for charging the VC battery 60 over the period 10:00-14:30, and discharging the VC battery 60 over the period 20:00-24:00.

The aim of the results depicted in Fig. 7 and Fig. 8 is to show how the proposed robust mathematical optimization program allocates fractions of the PV-battery systems power capacity to the voltage and frequency control services. Fig. 7 also illustrates the fact that PV-battery systems located in distribution networks with voltage problems cannot commit to provide a fixed reserve capacity (over the entire contracted period) and cannot commit to provide the same reserve capacity for the upward-FCR and downward-FCR. Therefore,

This article has been accepted for publication in a future issue of this journal, but has not been fully edited. Content may change prior to final publication. Citation information: DOI 10.1109/ACCESS.2020.3018086, IEEE Access

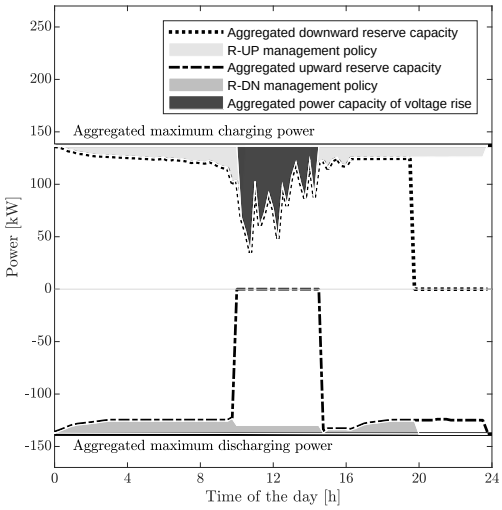

Fig. 7: Aggregated power capacities of the downward-FCR, upward-FCR, voltage rise, energy management policies of R-DN and R-UP batteries.

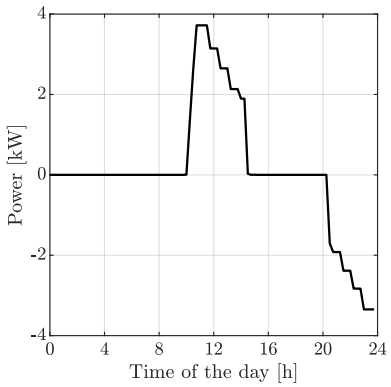

Fig. 8: Power capacity reserved for charging/discharging the VC battery 60.

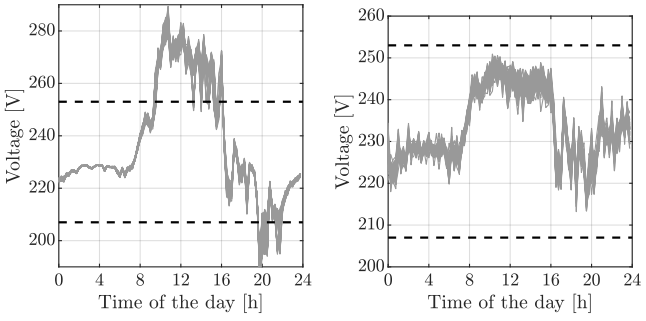

Fig. 9: (a) Voltage profiles of control node 60 with no control, (b) Voltage profiles of control node 60 with voltage and frequency control. The dotted lines show the maximum and minimum voltage limits

it is recommended for TSOs to design a new FCR auction, in which FCR capacity can be auctioned daily in the form of 15 minutes products. Additionally, the upward and downward reserves are recommended to be procured independently.

Voltage profiles are computed for the 10^4 scenarios without activating the control system. Fig. 9a shows voltage profiles of control node 60 (phase to neutral voltage). One can see that most of voltage profiles of different scenarios exceed

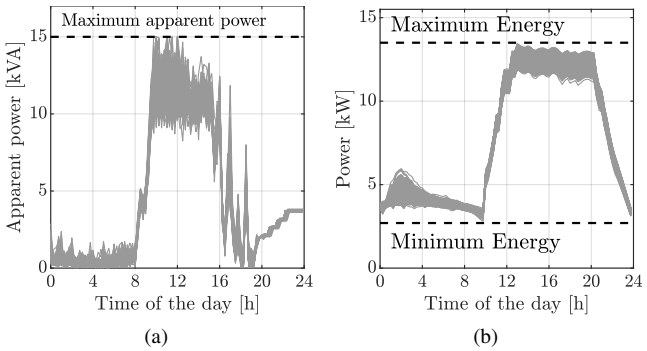

Fig. 10: (a) Apparent power magnitude of inverter 60, (b) Energy content of battery 60.

the voltage limits. When linear voltage control policies are applied, with frequency control enabled, it is noticed that the existing violations of voltage limits are eliminated for the 10^4 scenarios, which demonstrates the robustness of the proposed voltage control policies. Fig. 9b shows voltage profiles of control node 60 (at the end of the feeder VIII-X) after applying voltage control policies, with frequency control enabled.

Fig. 10a and Fig. 10b show, respectively, the apparent power magnitude of inverter 60 and energy content of battery 60 for all the scenarios. One can see that the capacity limits of the inverter and battery are respected for all the scenarios. The R-UP and R-DN energy management policies succeed in maintaining the energy content of battery 60 within limits while providing downward-FCR and upward-FCR, which demonstrates the robustness of the proposed energy management policies. To operate the control system sustainably, the control system starts to discharge the battery from 20:00 to reach a state of charge at the end of the day close to that of the start of the day.

The results presented in figures 9b, 10a and 10b validate the effectiveness of the robust mathematical optimization program to handle uncertainty. The constraints of the optimization problem are formulated based only on one scenario for the demand, PV and frequency (forecasted load/PV profiles and historical maximum/minimum frequency deviations), and the uncertainty model (presented in subsection V-A), nevertheless, the computed control policies are able to maintain operational limits of PV-battery systems and voltages for the 10^4 scenarios. This is one of the advantages of using robust optimization. In robust optimization, one does not need to formulate thousands of constraints for each time step, as in stochastic optimization, to handle uncertainties.

The offline computation takes around 155.6 minutes to solve the robust optimization problem (33a)-(33f). This is based on a workstation with an Intel Core i7-7700HQ CPUs (2.80 GHz) and 32 GB of RAM. This is an acceptable computation time, since the offline calculations run on a day-ahead basis. We would like to point out that the proposed control methodology is meant for a low voltage (LV) distribution network. A single LV network can have up to 150 nodes. Hence, we do not expect the proposed control methodology

to have scalability issues in such networks.

E. OPTIMALITY GAP

We compute upper bounds on the optimal solutions of the 10^4 scenarios by solving the robust optimization problem (33a)-(33f). We solve the dual problem (38a)-(38e) for the 10^4 scenarios to find the lower bounds. The optimality gaps of the different scenarios are computed by comparing the lower bounds to the upper bounds. Results show that the optimality gap of the proposed robust control methodology varies between 8% and 13% for the 10^4 scenarios, which is an acceptable optimality gap. We would like to remind the reader that obtaining an optimal solution is intractable. Hence, we trade-off optimality for computational tractability.

VII. CONCLUSION

In this paper, we complement previous work on PV-battery systems providing multiple services by designing a novel control system for residential PV-battery systems to provide simultaneously FCR service to their synchronous area and distributed voltage control service to their distribution network. Simulation results over 10^4 scenarios demonstrate the ability of the proposed control system to effectively regulate voltage profiles of the 120-node network and respond to the frequency deviations according to the pre-scheduled upward and downward reserve capacity profiles. Simulation results also validate our claim that upward and downward reserve capacity profiles of assets located in distribution networks with voltage problems cannot be fixed over the entire contracted period. Additionally, the results validate the proposed uncertainty model and control policies; the operational limits of voltages and PV-battery systems are respected for 10^4 realizations of the uncertain data.

We propose the following issues for future study:

- Robustness to communication failures and delays: Performance of the proposed distributed voltage control system depends on the availability and quality of the P2P communication between agents. The paper tests the performance of the proposed control system assuming communication performs perfectly. It is essential to quantify the impact of communication failures and delays on the performance of the proposed control system, and provide solutions to cope with communication failures and delays. These issues are out of scope of this paper, hence recommended for further research.
- Distribution networks with incomplete data: The prosed control methodology requires perfect knowledge of feeder characteristics, such as network topology and line segment impedances. The information that grid operators have about their networks is usually limited. Therefore, it is highly recommended for future research to augment the proposed control system with machine learning techniques to learn the topology and impedances of distribution networks.

REFERENCES

[1] Brent Wanner, IEA. Is exponential growth of solar PV the obvious conclusion? Available at: https://www.iea.org/commentaries/is-exponential-growth-of-solar-PV-the-obvious-conclusion. Accessed: 7 February 2020.

[2] International Renewable Energy Agency. Future of solar photovoltaic. https://www.irena.org/publications/2019/Nov/Future-of-Solar-Photovoltaic. Accessed: 05-05-2020.

[3] IEA (2019). Tracking energy integration: Energy storage , IEA, Paris. https://www.iea.org/reports/tracking-energy-integration. Accessed: 24-12-2019.

[4] M. Nijhuis, M. Gibescu, and J. Cobben, "Assessment of the impacts of the renewable energy and ICT driven energy transition on distribution networks," Renewable and Sustainable Energy Reviews, vol. 52, pp. 1003–1014, 2015.

[5] X. Wang, C. Wang, T. Xu, L. Guo, P. Li, L. Yu, and H. Meng, "Optimal voltage regulation for distribution networks with multi-microgrids," Applied Energy, vol. 210, pp. 1027–1036, 2018.

[6] A. M. Howlader, S. Sadoyama, L. R. Roose, and Y. Chen, "Active power control to mitigate voltage and frequency deviations for the smart grid using smart PV inverters," Applied Energy, vol. 258, p. 114000, 2020.

[7] A. Oudalov, D. Chartouni, C. Ohler, and G. Linhofer, "Value analysis of battery energy storage applications in power systems," in 2006 IEEE PES Power Systems Conference and Exposition. IEEE, 2006, pp. 2206–2211.

[8] S. J. Hossain, R. Bhattarai, M. Ahmed, S. Abdelrazek, and S. Kamalasadan, "Operational cost value assessment and value based stacked energy storage management for active power distribution systems," in 2017 IEEE Industry Applications Society Annual Meeting. IEEE, 2017, pp. 1–8.

[9] J. Engels, B. Claessens, and G. Deconinck, "Techno-economic analysis and optimal control of battery storage for frequency control services, applied to the german market," Applied Energy, vol. 242, pp. 1036–1049, 2019.

[10] H. Almasalma, S. Claeys, and G. Deconinck, "Peer-to-peer-based integrated grid voltage support function for smart photovoltaic inverters," Applied Energy, vol. 239, pp. 1037–1048, 2019.

[11] Elia, the Belgian TSO. FCR service design note. Available at: https://www.elia.be/en/electricity-market-and-system/system-services/keeping-the-balance/fcr. Accessed: 7 February 2020.

[12] T. Kern, S. Roon. New auction design for frequency containment reserve since 1 July 2019. Available at: https://www.ffegmbh.de/en/areas-of-expertise/scientific-analysis-of-system-and-energy-markets/106-electricity-market/892-new-auction-design-for-frequency-containment-reserve-since-1-july-2019-first-interim-results. Accessed: 10 March 2020.

[13] T. Thien, D. Schweer, D. vom Stein, A. Moser, and D. U. Sauer, "Real-world operating strategy and sensitivity analysis of frequency containment reserve provision with battery energy storage systems in the German market," Journal of energy storage, vol. 13, pp. 143–163, 2017.

[14] Elia, the Belgian TSO. Data download. Available at: https://www.elia.be/en/grid-data/data-download-page. Accessed: 10 January 2019.

[15] J. Fleer and P. Stenzel, "Impact analysis of different operation strategies for battery energy storage systems providing primary control reserve," Journal of Energy Storage, vol. 8, pp. 320–338, 2016.

[16] J. Mandel, J. Morris, H. Touati et al., "The economics of battery energy storage," Rocky Mountain Institute, 2015.

[17] E. Namor, F. Sossan, R. Cherkaoui, and M. Paolone, "Control of battery storage systems for the simultaneous provision of multiple services," IEEE Transactions on Smart Grid, vol. 10, no. 3, pp. 2799–2808, 2018.

[18] D. Wu, C. Jin, P. Balducci, and M. Kintner-Meyer, "An energy storage assessment: Using optimal control strategies to capture multiple services," in 2015 IEEE Power & Energy Society General Meeting. IEEE, 2015, pp. 1–5.

[19] O. Mégel, J. L. Mathieu, and G. Andersson, "Scheduling distributed energy storage units to provide multiple services under forecast error," International Journal of Electrical Power & Energy Systems, vol. 72, pp. 48–57, 2015.

[20] B. Cheng and W. B. Powell, "Co-optimizing battery storage for the frequency regulation and energy arbitrage using multi-scale dynamic programming," IEEE Transactions on Smart Grid, vol. 9, no. 3, pp. 1997–2005, 2016.

[21] Y. Shi, B. Xu, D. Wang, and B. Zhang, "Using battery storage for peak shaving and frequency regulation: Joint optimization for superlinear

gains," IEEE Transactions on Power Systems, vol. 33, no. 3, pp. 2882–2894, 2017.

[22] O. Mégel, J. L. Mathieu, and G. Andersson, "Stochastic dual dynamic programming to schedule energy storage units providing multiple services," in 2015 IEEE Eindhoven PowerTech. IEEE, 2015, pp. 1–6.

[23] J. Engels, B. Claessens, and G. Deconinck, "Combined stochastic optimization of frequency control and self-consumption with a battery," IEEE Transactions on Smart Grid, vol. 10, no. 2, pp. 1971–1981, 2017.

[24] D. K. Molzahn, F. Dörfler, H. Sandberg, S. H. Low, S. Chakrabarti, R. Baldick, and J. Lavaei, "A survey of distributed optimization and control algorithms for electric power systems," IEEE Transactions on Smart Grid, vol. 8, no. 6, pp. 2941–2962, 2017.

[25] K. S. Ayyagari, N. Gatsis, and A. F. Taha, "Chance constrained optimization of distributed energy resources via affine policies," in 2017 IEEE Global Conference on Signal and Information Processing (GlobalSIP). IEEE, 2017, pp. 1050–1054.

[26] R. A. Jabr, "Robust volt/var control with photovoltaics," IEEE Transactions on Power Systems, vol. 34, no. 3, pp. 2401–2408, 2019.

[27] ——, "Linear decision rules for control of reactive power by distributed photovoltaic generators," IEEE Transactions on Power Systems, vol. 33, no. 2, pp. 2165–2174, 2017.

[28] W. Lin and E. Bitar, "Decentralized stochastic control of distributed energy resources," IEEE Transactions on Power Systems, vol. 33, no. 1, pp. 888–900, 2017.

[29] H. Almasalma and G. Deconinck, "Robust Policy-Based Distributed Voltage Control Provided by PV-Battery Inverters," IEEE Access, vol. 8, pp. 124 939–124 948, 2020.

[30] K. E. Antoniadou-Plytaria, I. N. Kouveliotis-Lysikatos, P. S. Georgilakis, and N. D. Hatziargyriou, "Distributed and decentralized voltage control of smart distribution networks: Models, methods, and future research," IEEE Transactions on smart grid, vol. 8, no. 6, pp. 2999–3008, 2017.

[31] D. Kempe, A. Dobra, and J. Gehrke, "Gossip-based computation of aggregate information," in 44th Annual IEEE Symposium on Foundations of Computer Science, 2003. Proceedings. IEEE, 2003, pp. 482–491.

[32] A. Ben-Tal, A. Goryashko, E. Guslitzer, and A. Nemirovski, "Adjustable robust solutions of uncertain linear programs," Mathematical programming, vol. 99, no. 2, pp. 351–376, 2004.

[33] İ. Yanıkoğlu, B. L. Gorissen, and D. den Hertog, "A survey of adjustable robust optimization," European Journal of Operational Research, vol. 277, no. 3, pp. 799–813, 2019.

[34] K. Abdulla, J. De Hoog, V. Muenzel, F. Suits, K. Steer, A. Wirth, and S. Halgamuge, "Optimal operation of energy storage systems considering forecasts and battery degradation," IEEE Transactions on Smart Grid, vol. 9, no. 3, pp. 2086–2096, 2016.

[35] N. Efkarpidis, T. De Rybel, and J. Driesen, "Optimization control scheme utilizing small-scale distributed generators and OLTC distribution transformers," Sustainable Energy, Grids and Networks, vol. 8, pp. 74–84, 2016.

[36] M. E. Baran and F. F. Wu, "Network reconfiguration in distribution systems for loss reduction and load balancing," IEEE Power Engineering Review, vol. 9, no. 4, pp. 101–102, 1989.

[37] M. Farivar, L. Chen, and S. Low, "Equilibrium and dynamics of local voltage control in distribution systems," in 52nd IEEE Conference on Decision and Control. IEEE, 2013, pp. 4329–4334.

[38] J. Löfberg. Yalmip. Big-M and convex hulls. https://yalmip.github.io/tutorial/bigmandconvexhulls/. Accessed: 13-03-2020.

[39] D. Kuhn, W. Wiesemann, and A. Georghiou, "Primal and dual linear decision rules in stochastic and robust optimization," Mathematical Programming, vol. 130, no. 1, pp. 177–209, 2011.

[40] D. Bertsimas and F. J. de Ruiter, "Duality in two-stage adaptive linear optimization: Faster computation and stronger bounds," INFORMS Journal on Computing, vol. 28, no. 3, pp. 500–511, 2016.

[41] Cenelec, "European standard EN 50160 on power quality: Voltage characteristics of electricity supplied by public distribution networks," 2007.

[42] I. Richardson, M. Thomson, D. Infield, and C. Clifford, "Domestic electricity use: A high-resolution energy demand model," Energy and buildings, vol. 42, no. 10, pp. 1878–1887, 2010.

[43] J. Bright, C. Smith, P. Taylor, and R. Crook, "Stochastic generation of synthetic minutely irradiance time series derived from mean hourly weather observation data," Solar Energy, vol. 115, pp. 229–242, 2015.

[44] J. Löfberg, "Yalmip: A toolbox for modeling and optimization in matlab," in Proceedings of the CACSD Conference, vol. 3. Taipei, Taiwan, 2004.

[45] Mosek, APS. The MOSEK optimization software, 2018 (Version 9.0) [Software]. Available: https://www.mosek.com/.

[46] R. D. Zimmerman, C. E. Murillo-Sanchez (2019). MATPOWER (Version 7.0) [Software]. Available: https://matpower.org/.

HAMADA ALMASALMA earned the B.Sc. degree in electrical engineering from Birzeit University, Palestine, in 2011, the M.Sc. degree in smart grids from Grenoble Alps University, France, in 2015, and the Ph.D. degree in electrical engineering from the KU Leuven, Belgium, in 2020. He is now working as a researcher at the Flemish institute for technological research (VITO), Belgium. His main research interests are modeling and optimization applied to power system.

GEERT DECONINCK earned his M.Sc. degree in electrical engineering and his Ph.D. degree in engineering science from the KU Leuven, Belgium, in 1991 and 1996, respectively. He is a full professor at the KU Leuven and in the EnergyVille research center. His research focuses on robust distributed coordination and control, specifically in the context of smart electric-distribution networks. He is a fellow of the Institute of Engineering and Technology and cochair of the IEEE Systems, Man, and Cybernetics Society Technical Committee on Infrastructure Systems and Services. He is a Senior Member of the IEEE.